2018

STRATIGRAPHY AND ORGANIC GEOCHEMISTRY REVEAL PATTERNS OF LATE QUATERNARY PALEO-PRODUCTIVITY AT MONO LAKE, CALIFORNIA

Bailee Nicole Hodelka
University of Kentucky, baileehodelka@gmail.com
Digital Object Identifier: https://doi.org/10.13023/etd.2018.340

STUDENT AGREEMENT:

I represent that my thesis or dissertation and abstract are my original work. Proper attribution has been given to all outside sources. I understand that I am solely responsible for obtaining any needed copyright permissions. I have obtained needed written permission statement(s) from the owner(s) of each third-party copyrighted matter to be included in my work, allowing electronic distribution (if such use is not permitted by the fair use doctrine) which will be submitted to UKnowledge as Additional File.

I hereby grant to The University of Kentucky and its agents the irrevocable, non-exclusive, and royalty-free license to archive and make accessible my work in whole or in part in all forms of media, now or hereafter known. I agree that the document mentioned above may be made available immediately for worldwide access unless an embargo applies.

I retain all other ownership rights to the copyright of my work. I also retain the right to use in future works (such as articles or books) all or part of my work. I understand that I am free to register the copyright to my work.

REVIEW, APPROVAL AND ACCEPTANCE

The document mentioned above has been reviewed and accepted by the student's advisor, on behalf of the advisory committee, and by the Director of Graduate Studies (DGS), on behalf of the program; we verify that this is the final, approved version of the student's thesis including all changes required by the advisory committee. The undersigned agree to abide by the statements above.

Bailee Nicole Hodelka, Student

Dr. Michael M. McGlue, Major Professor

Dr. Edward Woolery, Director of Graduate Studies

STRATIGRAPHY AND ORGANIC GEOCHEMISTRY REVEAL PATTERNS OF LATE QUATERNARY PALEO-PRODUCTIVITY AT MONO LAKE, CALIFORNIA

THESIS

A thesis submitted in partial fulfillment of the requirements for the degree of Master of Science in the College of Arts and Sciences at the University of Kentucky

By

Bailee Nicole Hodelka

Lexington, Kentucky

Director: Dr. Michael M. McGlue, Pioneer Professor of Earth and Environmental Sciences

Lexington, Kentucky

2018

ABSTRACT OF THESIS

STRATIGRAPHY AND ORGANIC GEOCHEMISTRY REVEAL PATTERNS OF LATE QUATERNARY PALEO-PRODUCTIVITY AT MONO LAKE, CALIFORNIA

Mono Lake (CA) is a hydrologically closed lacustrine basin well-known for its paleo-shorelines, which record fluctuations in water level for the last deglacial and late Holocene. Mono Lake is a sentinel of California's water supply, situated in the rain shadow of the Sierra Nevada, a mountain range whose snowpack is a vital source of freshwater for urban and agricultural districts to the west and south. Recent droughts, floods, and wildfires show that California is threatened by climate change, but how these changes impact and get recorded by Mono Lake sediments remains poorly known. Here, we use a new radiocarbon-dated deepwater sediment core from Mono Lake to test the hypothesis that organic facies development is controlled by climate and limnological change. An integrated stratigraphic analysis of the core reveals seven lithostratigraphic units that track environmental changes from ~16-4 ka. When compared to available paleo-shoreline and shallow water core data, our results show that high amplitude lake-level fluctuations of the late Pleistocene produce different patterns of sedimentation and organic enrichment than lower-amplitude water level changes of the early and middle Holocene. The results have implications for understanding patterns of paleo-production and hydroclimate change at Mono Lake.

KEYWORDS: Stratigraphy, Sediment Cores, Organic Geochemistry, Hydroclimate, Paleo-Productivity

Bailee Nicole Hodelka

4/24/2018

STRATIGRAPHY AND ORGANIC GEOCHEMISTRY REVEAL PATTERNS OF LATE QUATERNARY PALEO-PRODUCTIVITY AT MONO LAKE, CALIFORNIA

By

Bailee Nicole Hodelka

Dr. Michael M. McGlue

Director of Thesis

Dr. Edward Woolery

Director of Graduate Studies

April 24th, 2018

Date

ACKNOWLEDGEMENTS

This thesis would not have been possible without the insight and direction of my adviser, Dr. Michael McGlue, as well as the other members of my committee, Dr. Frank Ettensohn and Dr. Dave Moecher. Key collaborators on this project were Dr. Susan Zimmerman, Dr. Guleed Ali, and Dr. Irene Tunno, whose work laid a foundation for this thesis.

I want to thank the Mono Lake Commission for their support of this project and the Mono-Inyo National Forest for supplying the permit. I also want to give a special thanks to Richard Niederreiter, Martin Niederreiter, and Joseph Lucas for their field assistance. I want to thank LacCore and their staff who helped with core curation and ICD's. I also want to thank the Brown-McFarlan travel fund, which allowed me to travel to conferences to present my research and obtain feedback. I also want to thank my family, friends, and lab-mates whose moral support was invaluable during this project.

TABLE OF CONTENTS

LIST OF TABLES

LIST OF FIGURES

CHAPTER ONE: INTRODUCTION

The Sierra Nevada region supplies California (western USA) with more than 60% of its developed water supply, which is utilized by ~25 million people and irrigates ~3 million acres of valuable agricultural land (Vicuna and Dracup, 2007; Sierra Nevada Conservancy, 2015). The modern hydrology of the Sierra Nevada is controlled by winter storms originating in the Pacific Ocean, which in many years form a heavy snowpack on the mountain peaks along the northeastern margin of California. As the snowpack melts in the spring and summer, it feeds streams which are diverted to fill reservoirs. However, from 2012-2016, California experienced its worst drought in more than 1200 years (Cook et al., 2009; Griffin and Anchukaitis, 2014). For the world's sixth largest economy, the lack of precipitation had a severe impact on the production of fruits, nuts and vegetables, as well as on people from the Central Valley to Southern California (Respaut, 2016).

Paleoclimate proxy records (i.e., from tree rings and speleothems) have shown that droughts are not uncommon in the Sierra Nevada, and in fact, there is evidence of longer and more severe "megadroughts", which usually last on the order of 20-40 years (Herweijer et al., 2007; Griffin and Anchukaitis, 2014), exist in the late Holocene record. Tree-ring chronologies from the 2014 growing season revealed that while the precipitation during the 2012-2014 drought was anomalously low, it was not outside the range of natural variability. Griffin and Anchukaitis (2014) suggested that the severity of the drought was exacerbated by the record high temperatures associated with anthropogenic emissions of greenhouse gases and enhanced evaporative demand. High temperatures likewise affect the North Atlantic Ocean, which some authors (i.e., Denton et al., 2006; Chiang et al., 2014; Cvijanovic et al., 2017) believe to be an important region

for global climate with teleconnections to precipitation and water availability in California. Recent sea-ice modelling (Cvijanovic et al., 2017) revealed that changes in North Atlantic and Antarctic sea-ice (loss or gain) shift the location and strength of tropical convection, which leads to changing storm tracks over California. If Arctic sea ice continues to decrease, as is expected during the next several decades due to greenhouse gas emissions and higher temperatures, these conditions will result in substantial wintertime warming and favor drying over California (Wang and Overland, 2009; Olsen et al., 2011; Pederson et al., 2016; Cvijanovic et al., 2017).

Although tree rings and speleothems are valuable archives of paleo-precipitation, they preserve limited paleoenvironmental information, making the nature and timing of the response of inland aquatic ecosystems (e.g., lakes, wetlands, and rivers) to hydroclimate change difficult to fully ascertain. Therefore, well-dated sedimentary records from lakes in the eastern Sierra Nevada may be vital archives for learning more about the impacts of changing hydroclimate on this region of critical importance to California's water supply. In particular, hydrologically closed lakes are renowned for their sensitivity to changes in water balance, and as such form keystone archives of paleoenvironmental information for a number of arid and semi-arid regions around the world (e.g., Laird et al., 1996; Davis and Moutoux, 1998; Lowenstein et al., 1999; Plazcek et al., 2006; Colman et al., 2007; Morrissey and Scholz, 2014). Therefore, hydrologically closed lakes hold great promise for improving our knowledge of climate and ecological transitions in the Sierras.

Mono Lake is a hydrologically closed basin located in the rainshadow of the eastern Sierra Nevada in northeastern California (Figure 1). A number of Great Basin

lakes, including Mono Lake, have proven to be highly sensitive recorders of climate variations, as they respond rapidly to changes in precipitation and runoff (Benson et al., 1990; Stine, 1990; Newton, 1994; Davis, 1999; Benson et al., 2003; MacDonald et al., 2008; Zimmerman et al., 2011; Noble et al., 2016; Ali, 2018; Zimmerman et al., in rev.). Through the recent research of Ali (2018), Mono Lake has an extremely well-dated paleo-shoreline record from ~25.0-12.0 ka that demonstrates a number of high-amplitude water-level fluctuations during the Last Glacial Maximum and the deglacial (Figure 2). In addition, the geomorphological and stratigraphic studies of Lajoie (1968) and Stine (1990), resulted in a detailed paleo-shoreline elevation history for Mono Lake for the past ~4000 yrs (Figure 3), which is also marked by high-frequency changes. Together, these datasets form arguably the most comprehensively dated late Quaternary paleo-shoreline history for any lake on Earth.

However, because ancient shoreline records are unavailable from ~12.0-2.0 ka, the water-level history from this interval must be ascertained from sediment cores collected from beneath the extant lake. Furthermore, very little is known about the paleolimnology of Mono Lake over the deglacial and Holocene; unlike the beautifully exposed Wilson Creek Formation (Zimmerman et al., 2011), outcrops of lake beds from the last ~12 kyr are rare in the basin. The existing paleo-shoreline records provide critical lake-level elevation context for interpreting changes in limnology, sedimentary processes, and paleo-productivity within Mono Lake using sediment cores. This convergence of data is highly unusual in Quaternary paleolimnology. For many long-lived lake basins, paleo-shorelines, which provide quantitative insights on water-level elevation and lake volume,

assuming that tectonic changes have not deformed or uplifted the basin margins, are poorly preserved (Cohen, 2003).

Sediment cores collected from deepwater depocenters are usually better preserved and may contain more continuous stratal records than shorelines. Core records can also be challenging to collect and reliably date, and individually they provide limited spatial perspective on paleoenvironment. In the few instances where both dated paloeshorelines and long sediment core are available (e.g., Bolivia's Salar de Uyuni, and the western USA's Great Salt Lake), the records show considerable complexity, most particularly in the timing and down-dip expression of highstands and lowstands (Baker et al., 2001; Get al., 2004; Placzek et al., 2006; Placzek et al., 2013; Baker and Fritz, 2015). Although marrying these types of data is often not feasible, the insights on lake level provided by paleo-shorelines can lead to better constraints on paleolimnological interpretation than using sediment cores alone.

The focus of this study is on a new ~11 m long, deepwater sediment core collected from the western embayment of Mono Lake (Figure 4). Previous attempts to extract long cores from Mono Lake have not been successful, due in part to an abundance of tephras found at relatively shallow depths in the basin's subsurface that are difficult to penetrate. In this study, that sampling challenge was overcome by using an UWITEC percussion piston-corer (Figure 5), which was able to collect both coarse tephra beds and fine-grained lacustrine deposits without altering or disturbing the stratigraphy. Prior successful attempts at coring Mono Lake have mostly focused on shallow-water regions of the western embayment due to the Paoha Island uplift (~250 yrs BP) (Figure 4), a mid-lake volcanic eruption, disrupted large swaths of the lake floor away from the shoreline

(Christensen et al., 1969; Stine, 1990; Newton, 1994; Benson et al., 2003; Colman et al., 2014; Zimmerman et al., in rev.).

In addition, shallow-water cores have the advantage of recovering sediments that potentially contain terrestrial plant macrofossils, particularly in areas near riverine inputs (Davis, 1999). The Paoha Island eruption uplifted and overturned previously deposited lake beds, generating a mudflow which spread out over vast areas of the lake floor. In order to obtain a well-preserved sediment core suitable for comparison with the available paleo-shoreline record, the coring campaign undertaken in this study leveraged the seismic survey of Colman et al. (2014), which used high frequency CHIRP technology to image the shallow seismic stratigraphy of Mono Lake and the extent of disruption from the Paoha Island uplift. The Paoha Island uplift generated an acoustically distinct mudflow deposit, which pinches out in the western embayment at a scarp feature in ~24 m water depth (Figure 4). Therefore, we collected our core in 18 m of water to avoid heavily disrupted strata. Another issue associated with shallow-water cores is stratal completeness; due to dynamic lake levels, the littoral zone has at times been subaerially exposed and reworked by waves over latest Pleistocene and Holocene time (e.g., Zimmerman et al., in rev.). A deepwater sediment core provides the best potential for a continuous sedimentary record that preserves fine-scale details of aquatic processes and basin environmental history.

The hypothesis underpinning this study is that organic-facies development over millennial time scales in Mono Lake is controlled by environmental and limnologic changes. This hypothesis was tested using the aforementioned deepwater sediment core, which provides a record that encompasses the late deglacial (~17-13 ka), the Pleistocene-

Holocene transition (13-10 ka), and the Holocene through ~4.2 ka. The main objectives of this study were to: (1) analyze the core stratigraphy, (2) generate a radiocarbon-based age model for the core, (3) perform a multi-indicator organic-facies analysis that included physical properties (magnetic susceptibility), elemental geochemistry (total organic carbon, total carbonate, total nitrogen, biogenic silica), and stable-isotope geochemistry ($\delta^{13}C_{ORG}$, $\delta^{15}N_{ORG}$), and (4) integrate and compare the results with paleo-shoreline records and existing shallow-water cores. The multi-indicator approach was used to deduce changes in primary productivity, as well as to reveal other processes (e.g., preservation dynamics, dilution; Bohacs et al., 2000) that affect organic enrichment of the lake sediments.

Although some insights on paleo-productivity at Mono Lake are available through studies of the modern lake and recent sediments (e.g., Newton, 1994; Jellison et al., 1996), this study is the first to consider these changes for the Pleistocene and Holocene, and to relate these patterns to lake level and regional paleoclimate. Our results show that organic facies development at Mono Lake is sensitive to water-level changes, but the influence of water-level changes varies with time. The results have implications for understanding the influence of climate change on aquatic ecosystems in the Sierra Nevada, which may aid in predicting future environmental changes, tipping points, and ultimately, implementing better water-management practices.

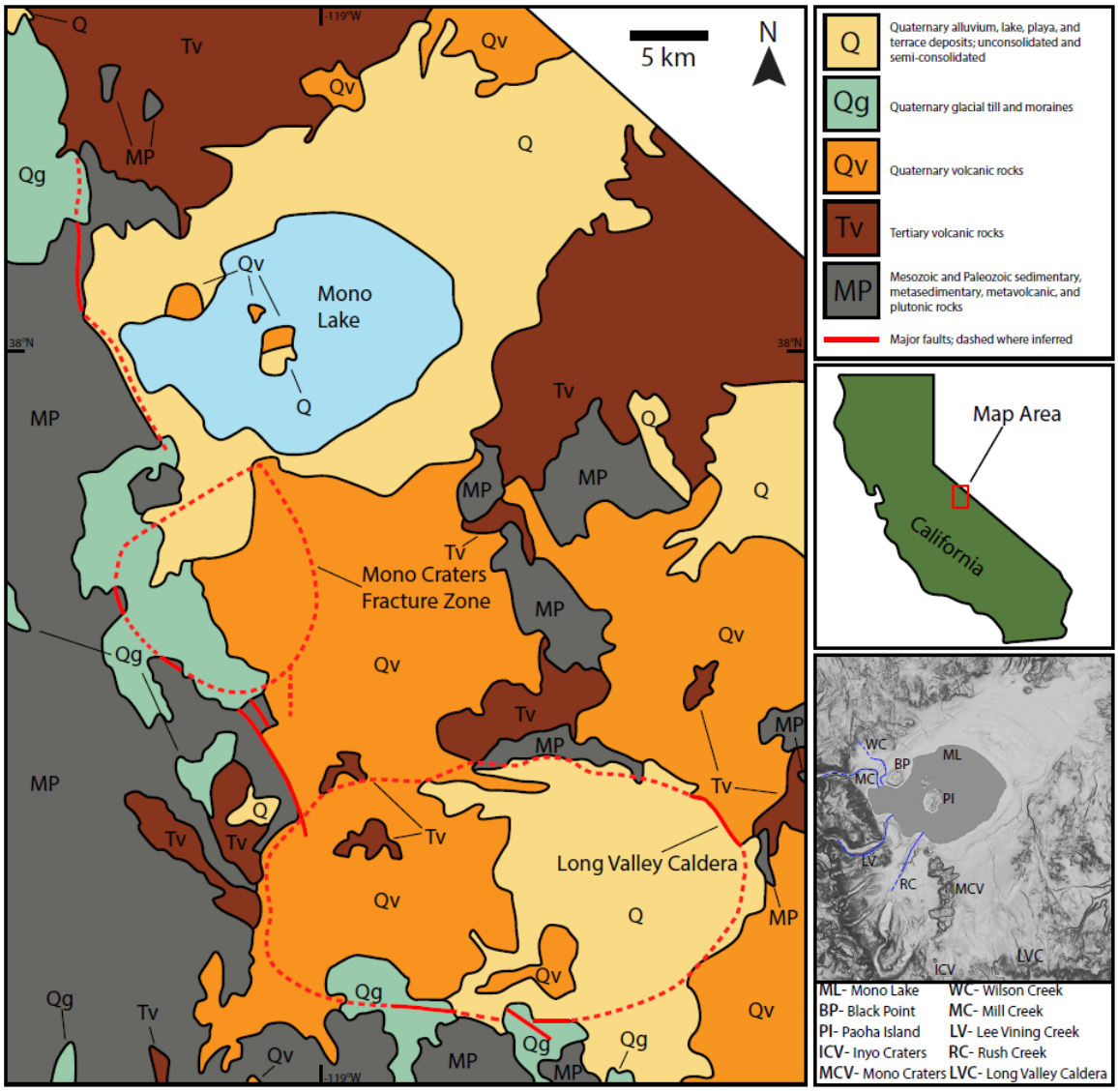

Figure 1: Left: Simplified geologic map of Mono Lake (modified from the California Geological Survey, 2010); Bottom Right: DEM (courtesy of S. Zimmerman) of Mono Lake showing the wide range of topography and locations of important features in the region.

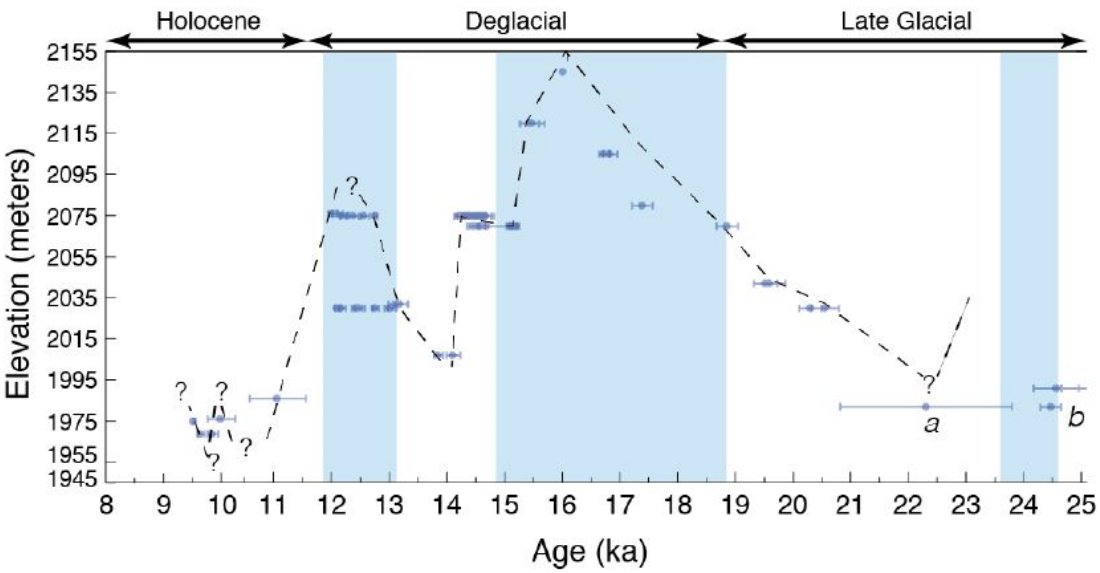

Figure 2: Mono Lake water level curve generated by Ali (2018). Curve was constructed by mapping and dating paleo-shorelines. Blue data points are U/Th and ^{14}C dates generated by Ali (2018). The blue shading on the graph coincides with periods of North Atlantic cooling; Heinrich Stadial 2 (24.5-23.5 ka), Heinrich Stadial 1 (18.6-14.7 ka), and Younger Dryas (12.9-11.7 ka). Note the magnitude of lake level fluctuations during this time were ≥ 75 m in elevation.

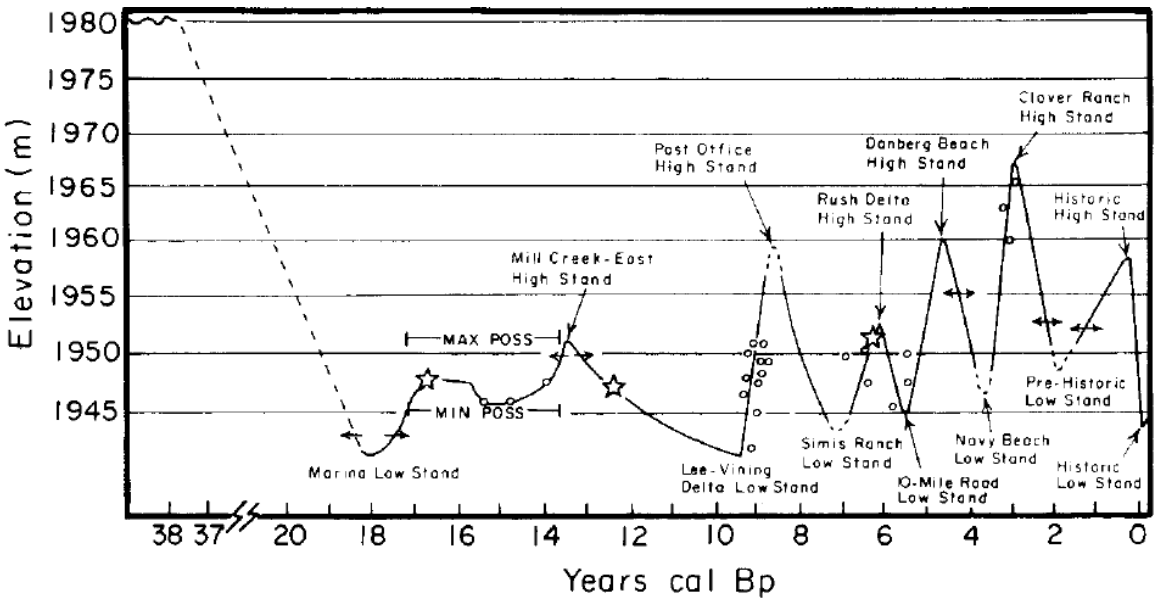

Figure 3: The late Holocene Mono Lake water level curve from Stine (1990). In the original publication the x-axis is mislabeled (should be years cal BP x 100). Note the high frequency changes in water level in the Holocene spanned ~25 m in elevation.

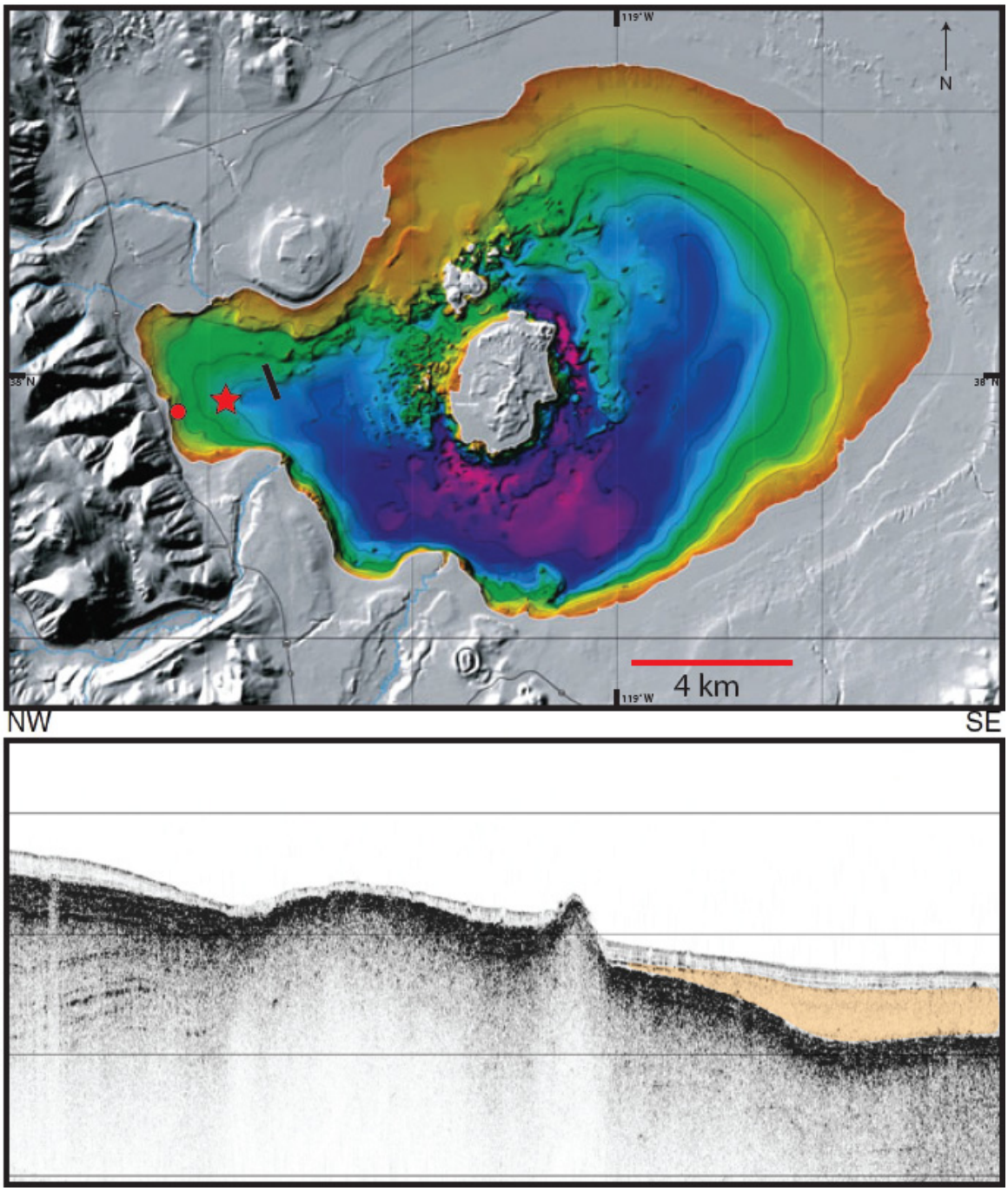

Figure 4: Top: Bathymetric Map of Mono Lake; red star is the location of the deepwater UWI15 core, red dot is the location of the shallow water BINGO 10/4A core, and black line is the seismic transect collected by Colman et al., 2014. Bottom: Modified seismic transect in the western embayment of Mono Lake; Orange unit is the S3 (Paoha Island Uplift) unit described by Colman et al., 2014; note how the S3 unit pinches out at a scarp like feature in the western embayment.

Figure 5: Photo of the UK-UWITEC percussion piston coring barge deployed on Mono Lake. Using this system, we were able to core through tephras and preserve delicate sedimentary structures.

CHAPTER TWO: BACKGROUND

2.1 Geologic Setting

The Mono Basin (~2070 km^2) is a broad, shallow structure located on the western edge of the Great Basin. The Mono Basin formed approximately 3-4 Mya as a result of regional warping and faulting (Christensen et al., 1969; Reheis et al., 2002). The basin is characterized by a wide range of topographic relief, from 1950 m.a.s.l. in the east to 3980 m.a.s.l. in the west (Davis, 1999) (Figure 1). The western edge of the basin is defined by the Sierra Nevada Batholith, which consists of Mesozoic granitic plutons with Paleozoic metasediments as roof pendants (Bateman, 1961). In the east, the majority of the Mono Basin consists of Pleistocene lake sediments, Holocene volcanic deposits, alluvium, and glacial outwash and till (Christensen et al., 1969; Davis, 1999). The north and south edges of the basin are formed by Tertiary volcanic hills and the rim of the Long Valley Caldera (Bailey et al., 1976; Hildreth, 2004) (Figure 1). The Pleistocene Wilson Creek Formation (Figure 6) is a prominent series of lacustrine silts composed of glacial flour that was eroded from the Sierra Nevada by valley glaciers, as well as 19 distinct tephra beds, which were erupted from the Mono Craters and deposited in Pleistocene Lake Russell (Benson et al., 1997; Zimmerman et al., 2006; Zimmerman et al., 2011; Vazquez and Lidzbarski, 2012).

The late Quaternary Mono and Inyo craters surround Mono Lake. The Mono and Inyo craters form a ~28 km volcanic chain that extends from Mono Lake to the Long Valley caldera (Figure 1). This chain is characterized by ~30 rhyolitic, dacitic, and rhyodacitic domes and one basaltic tephra cone (Black Point) near the north shore of Mono Lake (Kelleher and Cameron, 1990). The Mono Craters form an arcuate chain ~17

km long and are composed of chemically homogeneous rhyolite. The arcuate nature of the Mono Crater chain is believed to be related to a mylonitized ring-fracture system ~18 km in diameter (Figure 1). By comparison, the Inyo Craters form a straight but discontinuous ~11 km long chain of domes that are compositionally heterogeneous rhyolites and rhyodacites (Wood, 1977). This heterogeneity is believed to represent a mixing zone located along a north-south fissure system between the rhyolitic magma chamber beneath the Mono Craters and the rhyodacitic magma chamber beneath Long Valley (Bailey et al., 1976).

Volcanism from these craters produced tephras that provide the opportunity for detailed stratigraphic and age control in the region. The most well-known tephras in the region are the North Mono Tephra (~600-625 cal yr BP: Stine, 1987; Millar et al., 2006; Colman et al., 2014), the South Mono Tephra (~1.3 cal yr BP: Wood, 1977; Stine, 1987), Ash #1 ~12.9 ka (Benson et al, 1997) and Black Point (so-called "Ash #2"), but some debate still surrounds the dating of older tephras. For example, the Black Point ash has been dated at ~13,300 yr BP by Lajoie (1968), ~16,000 yr BP by Benson et al. (1998), and ~17,200 yr BP by Ali (2018).

2.2 Limnology

Mono Lake is the modern-day remnant of Pleistocene Lake Russell, which was the northernmost in a chain of pluvial lakes that flowed into the Owens River system (Newton, 1994). Today, Mono Lake is a hydrologically closed, saline (87‰), alkaline (pH = 10.0) lake located on the western boundary of the Basin and Range Province, within the rain shadow of the eastern Sierra Nevada (Stine, 1989; Newton, 1994). Mono

Lake covers ~160 km^2, averages ~17 m deep, and has a shoreline elevation of 1945 m above sea level (m.a.s.l.) (Jellison and Melack, 1993b).

Within Mono Lake, internal recycling of nutrients dominates the lake processes, and because Mono Lake is hydrologically closed, the recycling of nutrients is directly affected by environmental changes (Jellison et al., 1993). Mono Lake is typically a warm monomictic lake. The lake does not freeze over in the winter, and it becomes stratified in the spring and summer via the establishment of a thermocline, which breaks down in the fall and winter. This breakdown allows the dense bottom waters to mix with the surface waters, returning nutrients to the epilimnion. However, the water-column stratification is not static, and it can be affected by climatic variations such as the El Nino Southern Oscillation (ENSO). For example, in 1982 and 1983, heavy snowfall coupled with rainfall caused the Los Angeles Division of Water and Power (LADWP) to increase the amount of freshwater delivered to Mono Lake; this led to the establishment of meromixis, which lasted until 1988 (Jellison and Melack, 1993; Jellison et al., 1993; Zimmerman et al., 2011). During this time, Mono Lake did not experience turn-over, due to the presence of a strong chemocline, which marked the boundary between fresh surface waters and saline deepwater.

Mono Lake has no rivers that exit the basin, making it an endorheic lake (Wetzel, 2001). This condition of hydrological closure appears to have been the case for at least the last 50,000 yrs (Benson et al., 1990; Stine, 1990; Zimmerman et al., 2011; Vazquez and Lidzbarski, 2012). A number of small streams flow into the lake from the west, including Rush, Mill, and Lee Vining creeks (Figure 1). Delivery of snow-derived meltwater to Mono Lake from these and other small creeks is an important component of

the water cycle. Paleo-shoreline studies have shown that Mono Lake reliably reflects the amount of precipitation received by San Francisco, which demonstrates its viability as an archive of climate change (Stine, 1987).

2.3 Hydrology and Climate

Precipitation in the Mono Basin varies significantly with elevation. The lake receives an average of ~13 cm of precipitation per year, whereas Sierran crests can receive more than 127 cm (Stine, 1990; Newton, 1994; Davis, 1999). Precipitation for the region is winter-dominant and typically falls as snow; a 10-year average of station data from Lee Vining (2006-2015) shows that January received ~50 cm of precipitation, whereas July received 0.0 cm. Moreover, temperatures fluctuate widely, in January the average temperature is -1°C, while in July it is 21°C (Figure 7). However, in 2015 the Sierras received ~90 cm of precipitation, with the majority (~38 cm) falling in May, and average monthly temperatures ranged from 2°C in November to 20°C in August (Figure 7). This short-term variability highlights the importance of understanding the effects of climatic events such as atmospheric rivers and ENSO on the hydrology of the lake and more importantly, future hydrologic changes for the region.

Mono Lake is fed by three primary meltwater inflows from the eastern Sierra Nevada: Rush Creek, Mill Creek, and Lee Vining Creek (Figure 1). Under natural, unaltered conditions, these streams contribute ~80% of the estimated surface and ground water inflow to the lake (Stine, 1990). However, beginning in the 1940's, the majority of the runoff that fed these creeks was diverted into the Los Angeles Aqueduct, which caused the Mono Lake shoreline elevation to drop > 14 m (Stine, 1990; Stine, 1991; Newton, 1994; Benson et al., 2003). This drastic reduction in lake-water volume has

caused the salinity and alkalinity of the lake to nearly double due to evaporative concentration. Today, the ion chemistry of Mono Lake is dominated by Na^+, HCO_3^-, CO_3^{2-}, Cl^-, and SO_4^{2-} (Newton, 1994).

2.4 Aquatic Ecology

This diversion of meltwater sparked the "Mono Lake Controversy," one of the most highly publicized and protracted land-use conflicts in the western United States (Stine, 1991). Due to its unique water chemistry, the lake has a relatively simple food web comprised of coccoid chlorophytes, coccoid cyanobacteria, and several bacillarophytes (diatoms), which include *Nannochloris* sp., *Oscillatoria* sp., and *Nitzschia* sp. (Reed, 1977; Kociolek and Herbst, 1992; Wiens et al., 1993; Jellison et al., 1993; Newton, 1994; Herbst and Blinn, 1998; MacIntyre et al., 1999). These phytoplankton are consumed by zooplankton such as brine shrimp *(Artemia monica)* and brine flies *(Ephydra hians),* which form the resource base for more than 10^6 birds that occupy the lake during summer and early autumn (Weins et al., 1993).

The environment and vegetation of the Mono Basin includes high sagebrush desert, riparian woodland, pinon-juniper woodland, alkaline and freshwater marshes, and at higher elevations, montane forests, meadows, and freshwater lakes, which are frequented by many of the migratory and nesting bird species at Mono Lake (Wrege et al., 2006). However, the diversion of water to Los Angeles has altered the availability of aquatic habitats, configuration of the shoreline, and islands within the lake (Weins et al., 1993). The regression of the 1940's transformed the detached islands into peninsulas, which allowed predators such as coyotes to invade and disrupt prominent gull rookeries (Page et al., 1983; Stine, 1991). However, in 1994, the state board passed legislation to

restrict LADWP water diversions and maintain lake-level elevation at ~1948 m.a.s.l. (Koehler, 1995). Since then, lake-level has been a balance between diversions and climatic variations.

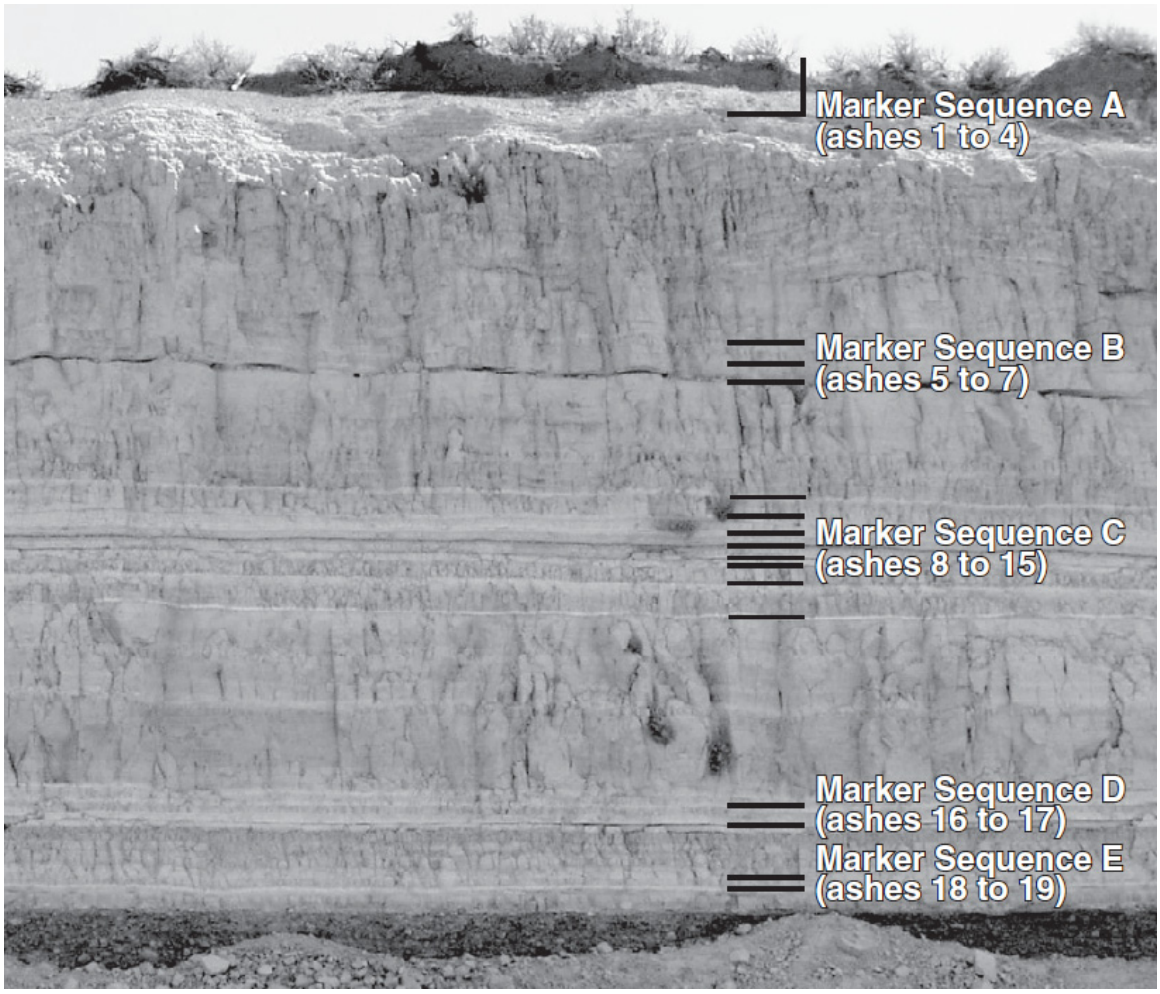

Figure 6: Type section of the Wilson Creek Formation. The Wilson Creek Formation contains 18 rhyolitic ashes and one basaltic ash which were grouped into five Marker Sequences (A-E) by Lajoie (1986). These marker sequences are useful for intrabasin correlation. Modified from Zimmerman, 2011.

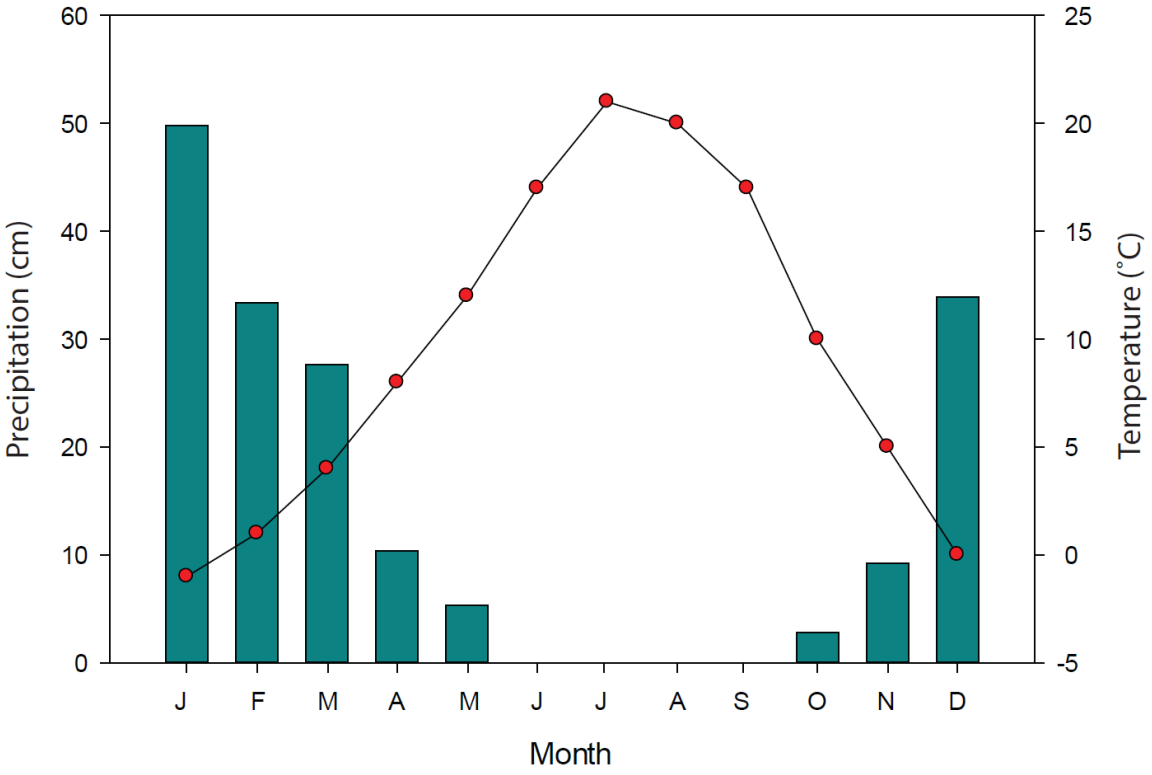

Figure 7: 10 year average of precipitation (blue bars) and temperature (red dots). Note that precipitation is winter dominant. Data was collected from the Lee Vining weather station and available online via NOAA.

CHAPTER THREE: METHODS

3.1 Core Collection

Sediment cores were collected from the western embayment of Mono Lake (Figure 4). The coring location was chosen based on an analysis of CHIRP seismic data from the study conducted Colman et al. (2014). That study identified four seismic stratigraphic units within the Mono Lake subsurface. The most important of the four units was named S3, which was interpreted to be a massive mudflow deposit caused by the uplift of Paoha Island. Unit S3 has a maximum thickness of ~18 m and thins radially away from Paoha. In the western embayment, S3 appears to pinch out at a scarp-like feature at 24 m water depth (Colman et al., 2014) (Figure 4). Therefore, the coring site was located at 37.99350˚N, -119.12540˚W in ~18 m water depth, to minimize the likelihood of encountering the mudflow deposit or disturbed strata caused by the uplift of Paoha Island.

This study utilizes three sediment cores collected using an UWITEC coring platform (Figure 5). The UWITEC can deploy both gravity cores and weighted percussion piston cores. We used an UWITEC gravity corer (a weighted PVC core liner) that was gently lowered to the sediment-water interface and allowed to settle into the lake floor under its own weight in order to collect the uppermost water-logged sediments at the site. Examination of the sediments revealed excellent (~100%) recovery without significant disturbance of delicate sedimentary structures.

Comparatively, the percussion piston corer uses a two-meter steel core barrel with PVC liners and a hydraulic piston. Using this device, the core barrel is hammered into the sediment past the piston with ~50 kg weight from the platform. The piston creates a

vacuum within the core barrel, which prevents sediment deformation and preserves delicate sedimentary structures (Guyard et al., 2011). To prevent sediment loss when the corer was extracted from the lake floor, a stainless steel orange-peel-style core catcher was affixed at the base of the corer. Using this technique, a sequential set of two-meter drives (UWI-Mono15-1C core) was collected to a total depth of ~18 m. However, because the piston takes up ~10 cm in the core barrel, and the core catcher may retain some sediment from the base of each drive, short gaps are associated with each drive. Therefore, it was necessary to collect an overlapping set of staggered drives (UWI-Mono15-1D core) in an adjacent borehole situated ~1 m from the initial borehole. Drives in this second borehole (1D) were arranged such that sediments from all gaps in the original borehole (1C) could be retrieved.

3.2 Core Correlation

In order to create a composite core from the overlapping drives in the adjacent boreholes, we used stratigraphic details and physical properties derived from initial core descriptions (ICDs) and multi-sensor core logger (MSCL) scans. The MSCL takes both density and magnetic susceptibility (MS) readings at 0.5 cm intervals. Each core was then split longitudinally, photographed at high resolution, and described using standard techniques at LacCore, the National Lacustrine Core Facility in Minneapolis (MN) (Schnurrenberger et al., 2003).

High resolution core photos were imported into Adobe Photoshop, processed, and correlated using distinct marker beds, sedimentary structures, and patterns in magnetic susceptibility and density derived from the MSCL. This process yielded a composite core that was ~1081 cm in length. Once the cross-correlation was complete, a

lithostratigraphic analysis was completed on the composite section in order to identify major units. Discrete 1 cm thick sediment samples (~5-10 cc) were collected approximately every 4 cm along the length of the core for total organic carbon (TOC), total inorganic carbon (TIC), total nitrogen (TN), $\delta^{13}C_{ORG}$, $\delta^{15}N_{ORG}$, and biogenic silica (BiSi) analyses. Exceptions to the sampling scheme occurred only in a few instances and are primarily related to the presence of coarse tephra beds.

3.3 Magnetic Susceptibility

High-resolution (0.5 cm) magnetic susceptibility (MS) readings were collected on the split cores at LacCore using a GeoTek MSCL-XYZ core workstation (Lascu, 2009). The section depths were converted to composite core depth in order to generate a comprehensive MS curve for the core. MS is often used as a proxy for detrital influx, with high MS values indicating greater delivery of terrestrial grains to the core site (Benson et al., 1998).

3.4 Radiocarbon

The materials selected for radiocarbon dating were plant macrofossils, charcoal, and pollen extracts. Bulk sediment samples were sent to the Center for accelerator mass spectrometry (CAMS) at Lawrence-Livermore National Laboratory (LLNL) to be processed for pollen using the procedure outlined in Tunno and Mensing (2017). Pollen was separated from each sample using flow-cytometry to remove any non-pollen organic material. Purified pollen samples, where concentrations were high, were combusted at high temperature, and the CO_2 generated was dated via AMS. Plant macrophytes and charcoal fragments were also collected for radiocarbon dating. These samples were typically found while sub-sampling the cores for other analyses. The samples were rinsed

with DI water, stored in glass vials, and shipped to CAMS, where they were pre-treated with standard acid-base-acid methods and dated by AMS. Another factor incorporated into the age model is the Black Point ash at the base of the core. The age of the Black Point ash is approximately 16.0 to 17.2 ka (Ali, 2018), thus a maximum age constraint is applied to the core for the age model generation using BACON; a Bayesian-based program that creates age-depth models for deposits (Blaauw and Christen, 2011).

3.5 Sediment Sample Preparation

Sediment sub-samples (*n=225*) were frozen in a -81˚C deep freezer and then placed in a Labconco FreeZone[12] lyophilizer for a minimum of 12 hours in order to remove pore water. Freeze-dried samples were crushed with an agate mortar and pestle, homogenized, and split for elemental and isotopic analyses.

3.6 Total Carbon (Organic Carbon and Inorganic Carbon)

Total organic carbon (TOC) values were obtained through LECO (total carbon) and carbonate coulometry (total inorganic carbon) as described by Meyers and Teranes (2001). TOC concentrations are used as a proxy for describing the abundance of organic matter in the sediments and TIC concentrations are used as a proxy for the abundance of carbonate (Cohen, 2003; Meyers, 2003). For total carbon (TC), freeze-dried and homogenized bulk samples were weighed in ceramic boats and then combusted in a LECO SC-144DR. The standards used were two synthetic carbon standards (502-030 and 502-630) and a carbonaceous shale (SARM-41). Precision for carbon analysis using the SC-144DR is ≤1% RSD or ±25 ppm, whichever was greater (LECO, 2008). To ensure complete combustion of the standards and samples, a catalyst Com-Cat (502-321) was added to each standard and sample that was analyzed. After the TC values were obtained,

the bulk samples were then analyzed for total inorganic carbon on a UIC CM5130 coulometer, which uses 0.1 M phosphoric acid to digest the inorganic carbon in the sample. Precision for the UIC CM5130 is ±0.2% if the carbonate standard (CM301-002) is within range. The TOC values were then calculated using the following equation: $TC - TIC = TOC$.

3.7 Stable Isotope Analysis

Samples for $\delta^{13}C_{ORG}$ analysis were digested overnight in centrifuge tubes with ~30 mL of 1 N HCl and ~20 mL of DI water. Following digestion, the samples were rinsed four times with DI water and centrifuged between each rinse. After the samples were rinsed, the acid-insoluble fraction was freeze dried and homogenized. The $\delta^{15}N_{ORG}$ analyses were performed on the bulk freeze-dried and homogenized sample which was not acid digested. All samples were analyzed for carbon and nitrogen isotopes using continuous-flow isotope-ratio mass spectrometry (EA-IRMS) at the University of Utah (UU).

At UU, the samples were analyzed using an elemental analyzer coupled to an isotope-ratio mass spectrometer through an open-split interface. During this process, the samples were dropped into a 1020°C Cr_2O_3 combustion reactor and pushed along by a helium carrier stream that was enriched with O_2. Under these conditions, the tin sample container ignites, raising the sample temperature to 1800°C, and forming H_2O, CO_2, and N_2. Any gas formed which contains halogens or sulfur is chemically removed and the remaining combustion products are sent into a 650°C Cu+ reducing reactor, where incomplete combustion products (NO_x, CO, etc.) are reduced and excess O_2 is removed. Water is then chemically scrubbed from the helium. The final product gases (N_2, CO_2)

are separated on a 3-m Porapak-Q packed gas chromatography column (80 mL min^{-1}, 40°C) before entering the IRMS via an open-split interface. Pure reference gases (ultra high purity grade N_2 and CO_2) enter the mass spectrometer at specified times to ensure proper mass calibration. C:N values were obtained using the % TOC from the aforementioned total carbon analysis and % Nitrogen values obtained from the isotopic analysis for $\delta^{15}N_{ORG}$. The values were then multiplied by 1.167 (Meyers and Teranes, 2001) to get the C:N atomic values, which are commonly used as a proxy to determine the source of organic matter. $TOC\% \div Nitrogen\ \% = C{:}N \times 1.167 = C{:}Natomic$

3.8 Biogenic Silica

Biogenic silica (BiSi) is used as a proxy for diatom productivity (Qiu et al., 1993). A total of 225 samples were analyzed for BiSi at Northern Arizona University. BiSi concentration was determined using the molybdate-blue spectrophotometry method described by Mortlock and Froelich (1989). Precision for this method is ±1.0 wt. %.

CHAPTER FOUR: RESULTS

4.1 Lithostratigraphy and Geochemistry

Seven different lithostratigraphic units were identified in the composite UWI15 core on the basis of physical properties and geochemical trends (Figure 8). Throughout the core, the sediments range from massive pumice tephra to finely laminated silts and muds (Figure 9). Depths for each unit are reported in centimeters below lake floor (cmblf).

4.2 Unit I (1081-1010 cmblf)

Located at the base of the core, Unit I is characterized by Black Point ash interbedded lacustrine silts, which are most likely responsible for producing the high-amplitude variability in MS that distinguishes the unit (Figure 8). The ash is medium-brown (10YR 4/3) with a velvety texture, and the beds are massive with irregular contacts, giving a heavily disrupted appearance. The interbedded silts are massive and light brownish-grey (10YR 6/2) in color (Figure 9). This unit has the lowest TOC (0.09-0.14 wt. %) and TIC (<0.25 wt. %) values in the core, whereas the BiSi concentrations (17.0-23.0 wt. %) are among the highest of any unit in this study. The $\delta^{13}C_{ORG}$ values range from -26.8‰ to -23.9‰, and exhibit a trend towards more positive values moving from the base towards the top of the unit. The $\delta^{15}N_{ORG}$ values range from -3.0‰ to 7.0‰; however, due to extremely low total nitrogen values (<0.1 wt. %), only three $C:N_{ATM}$ values were obtained and range from 9 to 13 (Figure 8).

4.3 Unit IIa (1010-802 cmblf)

Unit II is characterized by very dark bluish-grey (5PB 3/1) to black (N 2.5/1), finely laminated to thinly bedded muds, silts, and sands (Figure 9). The silts and sands

are responsible for producing high-frequency MS variability near the base of the unit that gradually declines moving up section (Figure 8). The sands are bright white granitic grains that occur either as thin beds or cm-scale lenses, which contrast with the medium-grey to black mm-scale laminated muds and silts. Unit IIa exhibits low-moderate TOC (mean = 0.9 wt. %) and TIC (mean = 0.5 wt. %) concentrations. The $C:N_{ATM}$ values in Unit IIa vary from 8-30, with an average value of ~13. The BiSi content (mean = 7.5 wt. %) is relatively low and invariant for this unit. The $\delta^{13}C_{ORG}$ values vary by ~8.0‰ in Unit II, and become increasingly negative towards the top of the unit, reaching values approaching -30‰. The $\delta^{15}N_{ORG}$ values range between 2‰ to 10‰ and generally decline moving up section (Figure 8).

4.4 Unit IIb (802-658 cmblf)

Unit IIb is characterized by very dark bluish-grey (5PB 3/1) to black (N 2.5/1) finely laminated to thinly bedded muds, silts, and sands (Figure 9). The MS values are lower than Unit IIa. Unit IIb contains a thick (~30 cm), massive black sand bed in the middle of the unit. The TIC concentrations are similar to Unit IIa and TOC values (mean = 1.0 wt. %) are only slightly higher on average. The $C:N_{ATM}$ values vary from 6-15, with an average value of ~12. The BiSi (mean = 10 wt. %) concentrations average ~2.0 wt. % higher than in Unit IIa. The $\delta^{13}C_{ORG}$ and $\delta^{15}N_{ORG}$ values remain relatively invariant throughout the unit with values that average -28‰ and 5‰, respectively (Figure 9).

4.5 Unit III (658-482 cmblf)

Unit III is characterized by finely laminated to thinly bedded muds and silts, which have a relatively low MS response (Figure 8). The muds are relatively fine-grained and dark reddish-grey (2.5YR 4/1) to olive-grey (5Y 5/2) near the top of the unit,

whereas at the base of the unit the muds are coarser, and blue-grey (10B 5/1) colors are more common (Figure 9). Unit III sediments have highly variable TOC values (0.5-9.0 wt. %) that generally increase upward towards the Unit IV contact. By contrast, TIC values (0.5-3.0 wt. %) are highly variable throughout the section, and show no discernible vertical trends. The BiSi values are likewise highly variable (3.0-19.0 wt. %), showing high amplitude changes without a clear vertical pattern. The $C:N_{ATM}$ values vary between 12-22 and increase toward the Unit IV boundary. The $\delta^{13}C$ values range between -28‰ to -23‰ and become increasingly positive up section. The $\delta^{15}N$ values become heavier up section and vary between 4‰ and 15‰ (Figure 8).

4.6 Unit IV (482-354 cmblf)

Unit IV is characterized by finely laminated silts and clays and thin beds of graded sands, which overall produce a low MS signal (Figure 8). The silts and clays are olive (5Y 5/4) and the sands are bluish-grey (5PB 5/1) (Figure 9). The unit has relatively invariant TOC and TIC concentrations, both of which average ~1.5-2.0 wt. %. The BiSi values vary widely (~5.0-15.0 wt. %) but generally decline moving towards the top of the unit. Similarly, the $C:N_{ATM}$ values decrease up section and vary between 12-17. The $\delta^{13}C_{ORG}$ values range from -25‰ to -23‰ and become more positive up section. The $\delta^{15}N_{ORG}$ values range from 3‰ to 6‰ and likewise increase up section (Figure 8).

4.7 Unit Va (354-286 cmblf)

Unit Va is characterized by dark blue-grey (5PB 4/1) to olive-brown (2.5Y 4/3) (Figure 9), finely laminated muds and silts with a low MS response. The TOC concentrations (mean = 2.0 wt. %) display a slight increase towards the top of the unit. The TIC values are highly variable and range from 0.4-5.0 wt. %. The BiSi values range

from 3.0-11.0 wt. % and show a slight decrease up section. The $C:N_{ATM}$ values show wide variability between 3-11, but no discernible vertical trend can be identified for the section. Muds from Unit V exhibit only minor variability in the $\delta^{13}C_{ORG}$ (-24‰ to -20‰) and $\delta^{15}N_{ORG}$ (4‰ to 8‰), with both isotopes becoming enriched towards the top of the unit (Figure 8).

4.8 Unit Vb (286-206 cmblf)

Unit Vb is characterized by olive-brown (2.5Y 4/3) (Figure 9) finely laminated muds and silts with a low MS response. TOC concentrations (mean = 3.0 wt. %) are ~1.0 wt. % higher than Unit Va, and values increase towards the Unit VI boundary. TIC concentrations are relatively invariant and range from 1.0-1.6 wt. %. $C:N_{ATM}$ values are likewise invariant and range from 13 to 16. The olive muds from Unit Vb exhibit slightly less variability in $\delta^{13}C_{ORG}$ (-24‰ to -21‰) and the $\delta^{15}N_{ORG}$ variability remains the same (4‰ to 8‰) as Unit Va (Figure 8).

4.9 Unit VI (206-62 cmblf)

Unit VI is characterized by dark olive-brown (2.5Y 3/3) to olive-grey (5Y 5/2), massive, sandy mud with massive light-grey (N 7/1) pumice tephra rubble (Figure 9), which produce a moderate to high MS response (Figure 8). Unit VI sandy muds exhibit TOC and TIC values from 0.2-4.0 wt. % and BiSi values from 3.0-11.0 wt. %. Below the tephra, the TOC and BiSi curves decline to low relative values, whereas an opposite trend characterizes the TIC curve. Above the tephra, TOC, BiSi, and TIC all increase, in some instances considerably (Figure 8). Comparatively, the $\delta^{13}C_{ORG,}$ $\delta^{15}N_{ORG,}$ and $C:N_{ATM}$ values become more positive both above and below the tephra. Of those three analyses, the $C:N_{ATM}$ values display the most variability, with values from 3-18, whereas the

$\delta^{13}C_{ORG}$ values (-24‰ to -20‰) are the least variable, and the $\delta^{15}N_{ORG}$ values display moderate variability from 6‰ to 16‰.

4.10 Unit VII (62-0 cmblf)

Unit VII is characterized by dark, finely laminated muds with a low MS response. The muds range from very dark greyish-brown (2.5Y 3/2) to greyish-green (5G 4/2), with green laminae most common near the base of the unit (Figure 9). The TOC values increase towards the top of the unit and range from 3.0-8.0 wt. %. The TIC values show a slight increase up section and range from 2.0-3.0 wt. %. Muds from Unit VII have widely varying BiSi concentrations (6.0-27.0 wt. %) but strongly decrease towards the top of the section. Unit VII muds have $\delta^{13}C_{ORG}$ values that range from -27‰ to -18‰ and $\delta^{15}N_{ORG}$ values that vary from 10‰ to 19‰; both isotope curves decline to more negative values towards the top of the unit. The $C:N_{ATM}$ values vary from 8-13 and shows a steady decline toward the top of the unit (Figure 8).

4.11 Age Model

The ages for dated material from UWI15 range from 3775-11110 ^{14}C years (Table 1). Pollen samples were collected every 50 cm and available ages range from 8140-12740 ^{14}C years from 3.5-9.5 m. Dates mentioned from this point forward have been calibrated (ka or cal yr BP) unless noted otherwise (^{14}C yrs). The identification and inclusion of the Black Point tephra constrains the age of the base of the core in the age model. Although not included in the age model, a candidate Ash 1 has been identified in Unit II. Work is currently underway to geochemically finger print the titanomagnetites to add more control points to the lower ~2 m of core. Sedimentation rates for the lower ~880 cm of core (Unit V to Unit I) are ~7 mm/yr. However, from the BACON age model (Figure 10),

it becomes apparent that sedimentation rates were markedly faster (~10 mm/yr) in the lower ~600 cm of core.

4.12 Modern Calibration Geochemistry

Modern calibration was performed on three sediment samples and 12 plant samples collected from a transect of Rush Creek from 1948 to 2019 masl (Figure 1). The modern sediments have an average $\delta^{13}C_{ORG}$ value of -26.3‰ and an average $\delta^{15}N_{ORG}$ of 3.9‰ (Table 2). The TOC values average 0.37 wt. %, whereas TIC values are below the detection level of the coulometer. The $\delta^{13}C_{ORG}$ values for plant samples range from -31.7‰ to -15.5‰ and $\delta^{15}N_{ORG}$ values range between -5.7‰ to 4.6‰. The $C:N_{ATM}$ values range from 11 to 64.

Table 1: Radiocarbon dates used in the age model generation for the UWI15 core.
* indicates dates not generated from this study but were provided by collaborators.

Lab #	Sample Name	Depth (cm)	Material	Age (^{14}C yrs)	Error (±)	Age (cal yr BP)	2-σ Range
175217	1D-1 Transition	96.6	Insect	1155	35	1070	982-1175
175215	1D-1 Transition	96.6	Plant	1180	60	1110	967-1260
177423	1C-2-1_54_55	205	Plant	3775	40	4150	3988-4286
	Triplet 1*	224	Tephra			4700	
	Triplet 2*	228	Tephra			5100	
	Triplet 3*	234	Tephra			5400	
176259	1C-2-2_45.7	296.3	Plant	5740	30	6540	6453-6634
173692	1D-2-1_67	307.4	Plant	6300	70	7225	7016-7416
173693	1D-2-2_3.5	314	Plant	6350	45	7285	7173-7416
173695	1D-2-2DUP_3.5	314	Plant	6150	40	7060	6943-7164
177425	1D-2-2_5.4_6.4	316.4	Plant	6620	110	7510	7427-7675
176260	1D-2-2_26_27	337	Charcoal	8850	100	9930	9610-10199
173694	1D-2-2_33.5	344	Plant	7070	70	7890	7739-8013
178075	1D-2-2_42.4	353	Pollen	8220	240	9150	8522-9680
118472	1D-2-2_43	354	Pollen	8140	240	9060	8458-9538
176261	1D-2-2_57.3	367.7	Plant	8610	180	9660	9155-10188
177392	1C-3-2_26.6	421.5	Plant	10070	570	11640	10187-13060
177393	1C-3-2_27.3	422.2	Plant	9910	410	11460	10298-12601
177394	1C-3-2_29.4	424.3	Plant	10010	570	11570	9957-13031
177395	1C-3-2_64.9	459.8	Plant	9400	70	10630	10411-11065
177396	1C-3-2_102.4	497.3	Plant	11110	600	12940	11217-14524
178076	1D-3-2_31	503	Pollen	10090	130	11670	11242-12115
178074	1C-4-2_39.5	653	Pollen	12650	390	14920	13758-16082
179010	1D-5-2_93.5_94.5	952	Pollen	12740	220	15110	14212-15802
	Black Point*	1082	Tephra		1900	17200	

Table 2: Modern geochemical calibration from sediment (T9) and plant samples collected on a transect up Rush Creek.

Sample	$\delta^{13}C_{ORG}$ (‰ VPDB)	$\delta^{15}N_{ORG}$ (‰ Air)	C:N (Atomic)	TOC (wt. %)	TN (wt. %)
T9-1-1B	-26.85	2.85	18	0.63	0.04
T9-7-3B	-26.81	3.17	15	0.38	0.03
T9-8-1B	-25.26	5.68	12	0.11	0.01
Artemisia arbuscula	-26.81	3.00	38	N/A	1.38
Purshia tridentata	-26.03	-2.29	35	N/A	1.58
Salix spp.	-28.51	-5.74	38	N/A	1.40
Eriogonum umbellatum	-26.41	1.18	31	N/A	1.61
Pinus jeffreyi	-24.26	0.98	64	N/A	0.86
Lupinus spp.	-28.81	2.41	11	N/A	4.27
Poaceae spp.	-15.47	1.38	30	N/A	1.60
Populus spp.	-27.52	-2.51	26	N/A	1.95
Chrysothamnus spp.	-26.70	-1.07	43	N/A	1.29
Rosa spp.	-28.62	-1.83	30	N/A	1.64
Salix spp.	-31.73	4.65	45	N/A	1.14
Typha spp.	-27.29	2.73	38	N/A	1.24

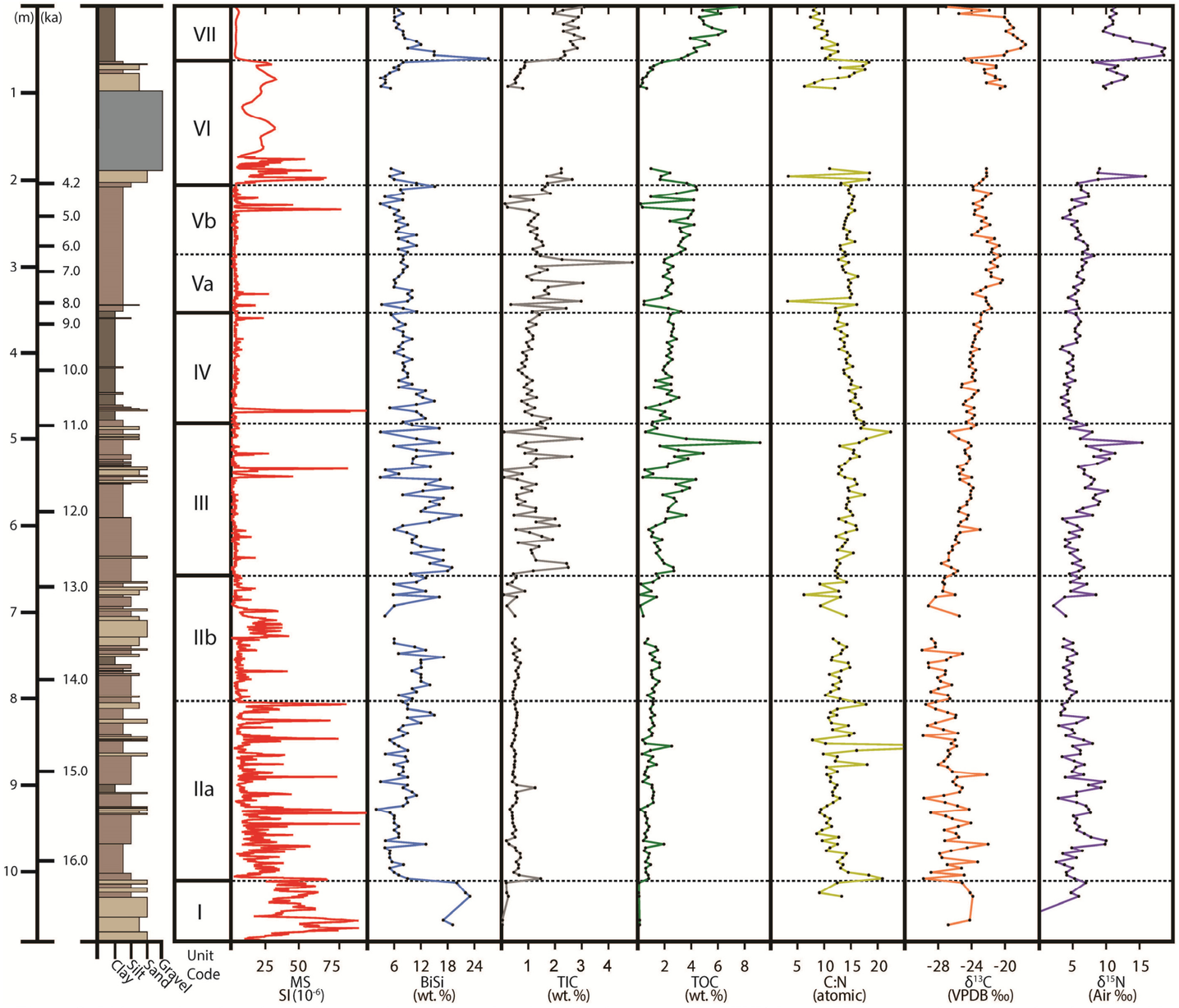

Figure 8: Lithostratigraphy, physical properties, and geochemistry for the composite UWI15 core. Units were chosen based on key transitions in physical and geochemical properties. From L-R: depth (m), age (ka), stratigraphic column (showing relative grain size), lithostratigraphic units and subunits, MS, BiSi, TIC, TOC, C:N, $\delta^{13}C_{ORG}$, and $\delta^{15}N_{ORG}$.

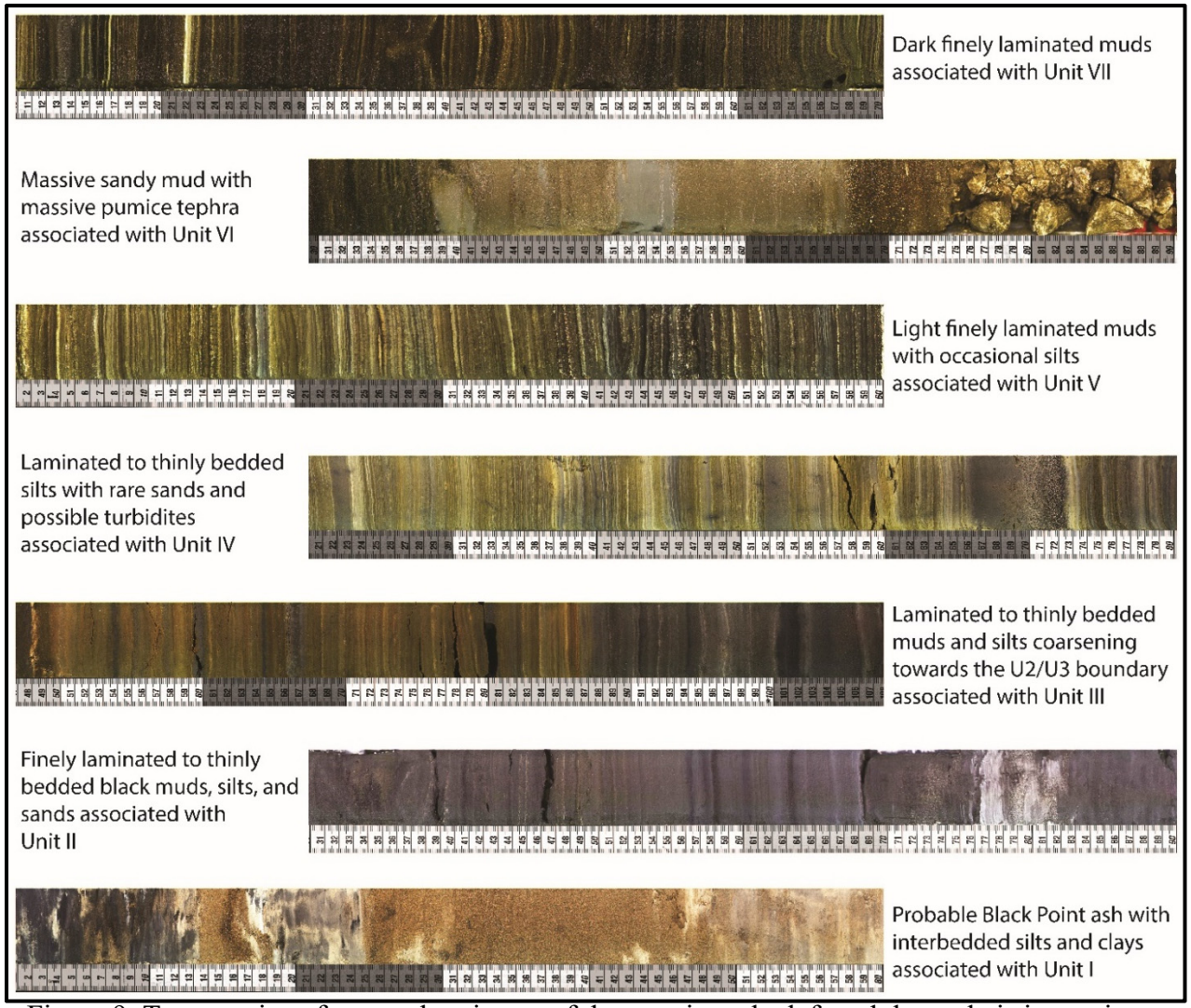

Figure 9: Type sections from each unit; top of the core is to the left and the scale is in centimeters. For Units II and V the sub-units (a and b) are not differentiated.

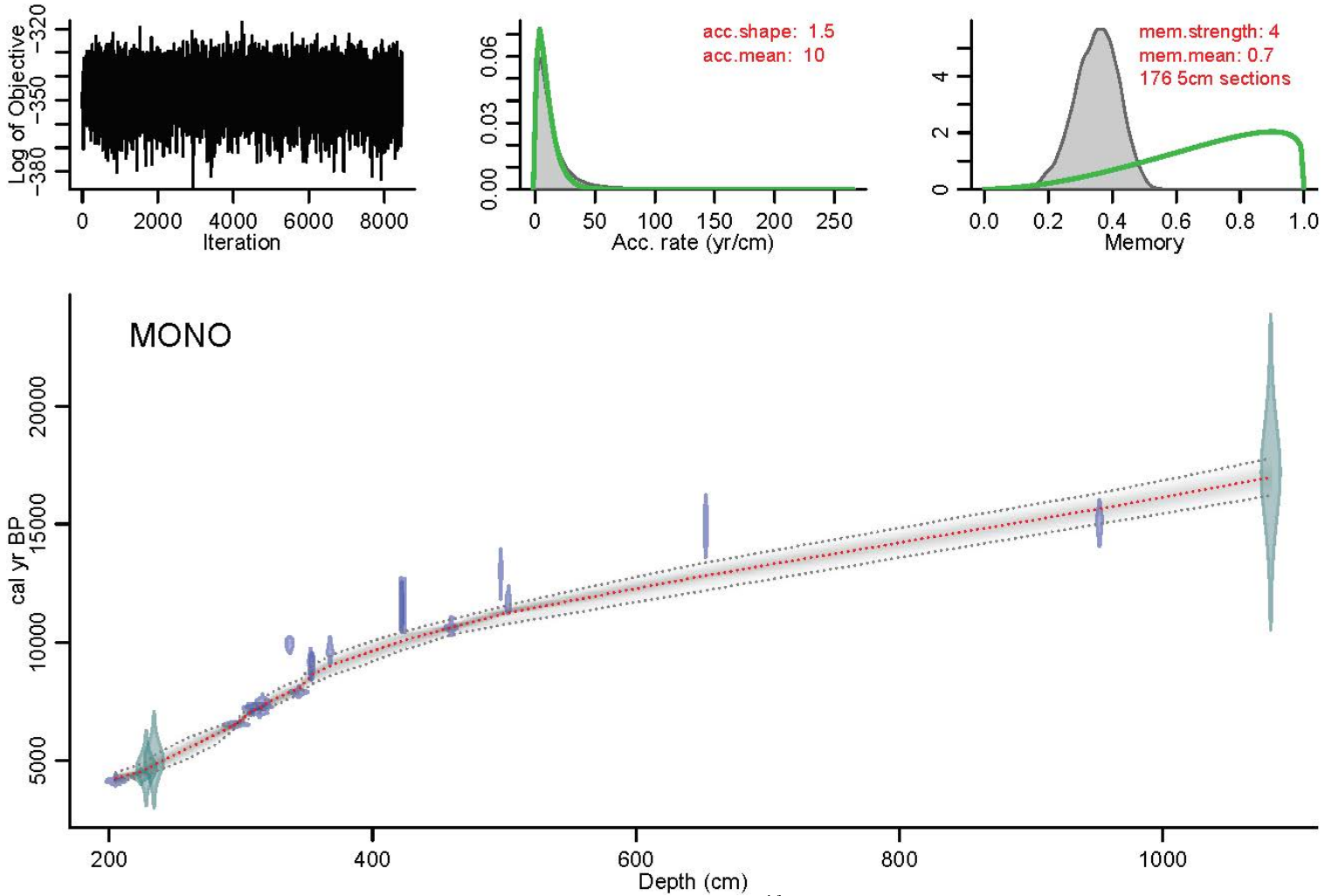

Figure 10: Age-depth model for the UWI15 core. The majority of ^{14}C dates are between 2.5 – 6.5 meters. The change in slope is due to an increase in sedimentation rates through the Pleistocene and into the Holocene. Blue-green bars are tephra dates that have been correlated to the UWI15 core; blue bars are dates generated in this study on plant macrophytes, pollen, and charcoal.

CHAPTER FIVE: DISCUSSION

5.1 Unit I (~16.9-16.2 ka)

At present, the chronology for Unit I is poorly constrained. The age model for Unit I is unconstrained by ^{14}C dated horizons and is defined by a pollen ^{14}C date at 952 cm in the overlying Unit II and an inferred date for Ash 2 deposits. Obtaining ^{14}C ages for Unit I has proven difficult, due to a lack of plant macrofossils and charcoal in this section of the UWI15 core. Research is underway to separate pollen using flow cytometry in order to add ^{14}C control points in the lower-most 2 m of core, as well as to fingerprint the Ash 1 candidate using the geochemistry of titanomagnetites (Marcaida et al., 2014; Zimmerman and Myrbo, 2015).

Unit I consists of ~71 cm of Black Point ash admixed with lacustrine silts and clays. The basaltic Black Point ash (Ash 2 of Lajoie, 1968) is one of the most easily identifiable eruptive deposits in the Mono Basin, and in our core, it expresses itself as a massive brown tephra with a velvet-like texture. Black Point ash disrupts the bedding of lacustrine silts and clays in Unit I. The Black Point ash is interpreted to be ~17.2 ± 1.9 ka (Ali, personal communication, 2018), which sets a maximum age for the lake sediments in this unit.

Due to the amount of ash in Unit I, the sampling interval for bulk geochemistry was coarse (*n=5* over 71 cm) and limited to the lake sediments. Unit I is characterized by relatively high MS, $\delta^{13}C_{ORG}$, and BiSi values, whereas TOC, TIC, $\delta^{15}N_{ORG}$, and $C:N_{ATM}$ are low (Figure 8). Unit I exhibits the lowest TOC concentrations (mean = 0.11 wt. %) and the lowest $\delta^{15}N_{ORG}$ values (mean = 2.0‰) found in the core. Typically, negative or zero values of $\delta^{15}N_{ORG}$ are attributed to a strong component of nitrogen-fixing

cyanobacteria in the organic-matter pool (e.g., Talbot, 2002; Brenner et al., 1999), though blue-green algae were not observed on smear slides from this interval.

The paleo-shoreline mapping and geochronological study of Ali (2018) suggests that a major deglacial transgression and highstand occurred in Mono Lake from ~18.5-16.0 ka, following a lowstand during the last glacial maximum (Figure 2). Thus, lake levels may have been high during the deposition of Unit I sediments. Although disrupted by the eruption of Black Point, we interpret that Mono Lake was a moderately productive aquatic ecosystem at this time, based on the limited geochemical evidence available, in spite of the low TOC concentrations, which suggests the possibility of an oligotrophic lake with limited nutrient supply. Smear slides from Unit I contained minor amounts of diatoms and amorphous organic matter, which is consistent with a lacustrine paleoenvironment with diverse algal composition.

BiSi concentrations are very high (mean = 20 wt. %) in Unit I, which notionally reflects elevated diatom productivity (Meyers and Lallier-Verges, 1999; Cohen, 2003; McFadden et al., 2004; McGlue et al., 2012). We anticipated a larger presence of diatoms on smear slides as a result of the BiSi concentrations; this disparity may be the result of partial dissolution of volcanic glass during the alkaline dissolution phase of the analysis. Nonetheless, the presence of diatom microfossils on smear slides confirms that Mono Lake was a suitable habitat for a diatom flora during Unit I time. Evidence in support of this interpretation comes from low $C:N_{ATM}$ values (mean = 11), and enriched $\delta^{13}C_{ORG}$ (mean = -25.0‰). According to Meyers (2003), $C:N_{ATM}$ values for lake algae are commonly between 4-10, whereas vascular land plants have C:N values ≥ 20. A mean $C:N_{ATM}$ value of 11 for Unit I suggests that algae were the dominant source of organic

matter during this time. The carbon isotopes are consistent with high relative rates of photosynthesis, which would serve to deplete ^{12}C from the water column and lead to isotopically heavy organic matter (Cohen, 2003; Meyers, 2003).

Magnetic susceptibility peaks are prominent in Unit I, and the Black Point ashes are characterized by some of the highest MS values in the UWI15 core (Figure 8). High MS values also characterize the lacustrine deposits in Unit I, which suggests that the low TOC concentrations may be explained by dilution or elevated sedimentation rates (e.g., Benson et al., 1998b; Noble et al., 2016). Unit I contains several very thin (<0.5 cm) graded silt beds, which we interpret to be the product of dilute turbidity currents that passed over the core site. However, it remains unclear if the turbidity currents occurred as a result of the sub-aqueous Black Point eruption (Benson et al., 1990), seismic activity that may have preceded the eruption, or pore pressure instabilities in the western embayment generated by lake-level changes.

We interpret that Mono Lake water chemistry was relatively dilute (~16.9-16.2 ka), based on the very low TIC concentrations in the lake deposits and the virtual absence of carbonate on smear slides. Carbonate precipitation in lakes is dominantly controlled by the availability of CO_2 in the water column (Cohen, 2003). The mechanisms that remove CO_2 and facilitate carbonate precipitation include, but are not limited to: (a) photosynthesis by lake margin macrophytes and algae, (b) CO_2 degassing, such as the discharge of supersaturated spring waters into the lake, (c) temperature changes that favor higher rates of evaporation, and (d) increasing salinity (Cohen, 2003). In a number of Great Basin paleo-lake studies, TIC concentrations were low during transgressions and lake-level highstands (Benson et al., 2003). Since the hydrologic inflows to Mono Lake

originate in the Sierra Nevada range, and weathering via hydrolysis reactions attack feldspars, the stream waters entering the lake contain a high ratio of HCO_3^- to dissolved Ca^{2+} (Garrels and Mackenzie, 1967).

Normally, in an evaporative, hydrologically closed lake, HCO_3^- and Ca^{2+} are removed in proportion by the precipitation of $CaCO_3$. However, Mono Lake is Ca^{2+} limited and an influx of freshwater carrying Ca^{2+} would cause the lake to precipitate $CaCO_3$ (Jones and Deocampo, 2003). Thus, if Mono Lake were transgressing or at highstand, the TIC concentrations in offshore strata might be predicted to be high, due to the abundance of Ca^{2+} in the water column, but due to the limited number of samples in Unit I and the dominance of the Black Point ash, it is most likely that samples from this interval have been diluted by siliciclastics. Moreover, an ostracode analysis completed by Forester (1987) showed that the Wilson Creek Fm., encompassing the Black Point ash (Marker Sequence A) (Figure 6) and associated lake deposits, contains a faunal assemblage consistent with dilute-water chemistry and high TIC concentrations, which supports the interpretation of high water levels at Mono Lake during Unit I time.

5.2 Unit II (IIa ~16.2-14.2 ka; IIb ~14.2-12.9 ka)

The geochronology for Unit II is constrained by a ^{14}C date at 952 cm and another ^{14}C control point just above the upper Unit II contact at ~653 cm (Table 1). The candidate Ash 1 horizon is present in Unit IIa and was selected on the basis of its thickness and stratigraphy (Zimmerman, personal communication, 2017). Lajoie (1968) describes Ash 1 as a white to light-grey rhyolitic ash and lapilli, overlain and underlain by light-grey laminated silts consisting of rhyolitic glass shards and ostracodes. In the UWI15 core, Ash 1 is similarly bounded by lacustrine silts, is light-grey in color and ~5 cm thick.

Through the geochemical finger printing of titanomagnetites, Marcaida et al. (2014) found that Ash 1, unlike some other rhyolitic ashes in Mono Basin, contains substantial amounts of iron. In the UWI15 core, preliminary x-ray fluorescence scans exhibit a significant iron peak at the stratigraphic level of the Ash 1 candidate, which suggests the potential for a positive geochemical correlation. The paleo-shoreline and stratigraphic analysis of Ali (2018) constrains the minimum age of Ash 1 to ~15.1 ka.

Unit II consists of finely laminated to thinly bedded black muds and silts with interbedded white-grey granitic sands. This unit is characterized by high amplitude variability in MS, BiSi, $\delta^{13}C_{ORG}$, $\delta^{15}N_{ORG}$, and $C:N_{ATM}$ (Figure 8). By comparison, the concentrations of TOC and TIC in Unit II are relatively low and invariant. The $C:N_{ATM}$ values are notably high in this unit, achieving values > 20 in several horizons. We interpret these high $C:N_{ATM}$ values to reflect important contributions of terrestrial vegetation to the organic-matter pool of Mono Lake at the time of deposition (Meyers and Lallier-Verges, 1999) (Figure 11). The delivery of terrestrial organic material was most likely facilitated by rivers, given the position of the UWI15 core in the western embayment (Figure 1). However, the $C:N_{ATM}$ does not reveal if the terrestrial organic matter was transported to the core site at lake-level lowstand by subaqueous hyperpycnal flows or at highstand via gravitational settling.

Hyperpycnal flows associated with river plumes laden with sediment can transform into turbidity currents, which move detritus and terrestrial organic matter along the lake floor to deepwater (Stine, 1990). By contrast, gravitational settling of terrestrial organic matter takes advantage of hydrodynamic sorting, which keeps low-density terrestrial organic matter in suspension for long time periods, allowing for wind-driven

currents to spread the material over a wide area, including offshore. This process has been implicated for explaining elevated deepwater C:N data in other large lakes (Meyers, 2002; Ellis et al., 2015). We favor the influence of low-density turbidity currents as the dominant process delivering terrestrial materials to the UWI15 core site in Unit II. Evidence in support of this interpretation comes from the MS data. The high amplitude MS response of Unit IIa suggests a considerable influx of magnetic grains offshore during this time, and cm-scale graded silt and sand beds in this interval are consistent with deposition via turbidity currents (Stine, 1990; Benson et al., 1998; Osleger et al., 2008; Noble et al., 2016) (Figure 12).

Notably, the paleo-shoreline analysis conducted by Ali (2018) makes clear that an important regression began in the Mono Basin after ~16 ka, following the large deglacial highstand. As a result, we interpret that the influence of turbidity currents was the direct result of falling lake levels, riverine incision, and the collapse of delta fronts. This interpretation is supported by the carbon-isotope data. Unit II is characterized by some of the most negative $\delta^{13}C_{ORG}$ values of the late Pleistocene-Holocene sedimentary package, and modern analog data suggest that this can be explained by the influence of deltaic processes (Table 3).

Modern sediments and live plants collected from Mono Lake's western embayment deltas exhibit mean $\delta^{13}C_{ORG}$ values of ~ -26.4‰, whereas the $\delta^{13}C_{ORG}$ chemostratigraphy of Unit II has a similar mean of ~ -26.9‰. As discussed by Cohen (2003), $\delta^{13}C_{ORG}$ in lakes is primarily controlled by the carbon-isotope composition of dissolved inorganic carbon (DIC) within the water column, as well as by contributions to the organic-matter pool from allochthonous sources in the watershed. Notably, a modern

riverine signal is not obvious in the geochemistry of recent muds from Mono Lake, and the three deltas which build into Mono Lake's western embayment today are ~7.8km, ~2.6km, and ~2.3km from the UWI15 core site (Figure 4). The research of Stine (1990) clearly shows that regressions on the order of decimeters in Mono Lake trigger rapid down-cutting of the eastward-flowing Sierran streams, and we interpret that similar incision and deltaic progradation most likely accompanied the regression identified by Ali (2018) for the deglacial. Lowstand deltas are a common phenomenon in large tectonic lake basins that influence deepwater stratal architecture, sedimentology, and organic matter composition (McGlue et al., 2006; Shanahan et al., 2006).

The enriched $\delta^{15}N_{ORG}$ values for Unit IIa suggests either a shift in the phytoplankton assemblage and subsequent drawdown of a limited DIN pool, or the volatilization of ammonia at relatively high pH, which causes a strong enrichment in ^{15}N. Talbot and Johannessen (1992) identified this process in the deglacial sedimentary record of tropical Lake Bosumtwi, and suggested that it was driven by a decline in lake level associated with higher aridity. Given the low TIC values for Unit IIa and high lake levels indicated by Lajoie (1968) and Ali (2018), it seems unlikely that Mono Lake was hypersaline, which favors a shifting algal composition to explain the nitrogen isotope data.

Bohacs et al. (2000) noted that organic richness in lake deposits reflects the balance among primary production, microbial decomposition, and processes of dilution. Low and invariant TOC concentrations throughout Unit IIa suggest that rates of primary productivity were potentially low during the regression and lake-level lowstand. However, the high-amplitude MS variability, along with elevated $C{:}N_{ATM}$ and $\delta^{13}C_{ORG}$

values, are consistent with an important role for processes of dilution influencing organic-facies development in Unit IIa time. Paleo-shoreline mapping and the stratigraphy and geochemistry of the Wilson Creek Formation strongly suggest that Mono Lake has been hydrologically closed for at least the last million years (Lajoie, 1968), and a lowstand during the deglacial is likely to have concentrated the remnant lake water and increased salinity.

Jellison et al. (1996) suggested that higher salinity may abate microbial processes that destroy organic matter in Mono Lake. Those authors used geochemical data from sediments deposited over the last ~170yrs that showed a positive correlation between salinity and sedimentary TOC to make their interpretations. This relationship does not appear to be important during Unit IIa time however, as TOC concentrations generally remain under 1.0 wt. % throughout the unit. It seems therefore likely that Mono Lake's western embayment was relatively fresh, even during low water levels due to the establishment of a chemocline. Moreover, the establishment of a freshwater cap in Mono Lake during this time could have facilitated the deposition of ungraded sand pods and lenses observed throughout Unit IIa and IIb via ice rafting (i.e., Zimmerman et al., 2011b).

Decomposition of organic matter at the sediment-water interface could have influenced the TOC concentrations in Unit II, but the presence of fine laminations and black (reduced) sediments argue against a permanently oxidized lake floor that was heavily reworked by microbes and bioturbating benthos. Therefore, low TOC concentrations are most likely influenced by the delivery of siliciclastic detritus to the core site from both lowstand deltas and ice rafted debris. Mean BiSi concentrations (8.0

wt. %) suggest diatom productivity was low during Unit IIa time, with a transition to slightly higher mean values (10.0 wt. %) in Unit IIb. In concert with MS data and core sedimentology, it is possible that algal productivity was limited by a turbid water column due to sediment laden runoff and reduced light penetration. Benson et al. (2003b) interpreted that similar processes affected productivity in Owens Lake, and Ali (2018) noted that turbidity may have constrained the depth of the photic zone at Mono Lake particularly when glaciers were actively eroding the eastern Sierra Nevada at this time.

The stratigraphy and geochemistry of Unit IIb (~14.2-12.9 ka) differs from underlying deposits, with sharp MS spikes disappearing, $\delta^{15}N_{ORG}$ values become more negative (mean = 5.0‰), and mean BiSi concentrations increasing by ~3.0 wt. % (Figure 8). Unit IIb also contains an unusual package of black, thickly bedded, vitreous sand; the origin of this deposit remains unknown but x-ray diffraction reveals its composition is dominantly quartz. We interpret that these different chemostratigraphic patterns were driven by climate change that began after ~14.2 ka, which led to a lake level lowstand associated with the onset of the Bolling-Allerod (~14.5-12.9 ka), a climate interval that marks the end of the last glacial period (Weaver et al., 2003). The onset of the Bolling-Allerod (B-A) was driven by a ~40 ppm increase in atmospheric CO_2, strengthening of the Atlantic meridonial overturning circulation (AMOC), and the subsequent release of heat stored in the ocean (Liu et al., 2009; Obbink et al., 2010; Shakun et al., 2012).

In the Eastern Sierras, the B-A has been characterized as a warm interglacial interval (Benson et al., 2003; MacDonald et al., 2008; Nowak et al., 2017). Paleo-shoreline analyses for this time (Figure 2) suggest that Mono Lake levels were falling (Ali, 2018), which is similar to observations from geological archives from Owens Lake

and Lake Bonneville (Oviatt, 1997; Benson et al., 1997). Furthermore, a pollen record from an Owens Lake sediment core and a vegetation analysis performed on woodrat middens near Pyramid Lake show a significant change in flora during the B-A, with woodlands being replaced by shrubs (Mensing, 2001; Nowak et al., 2017). These regional datasets are consistent with the physical properties and geochemistry of Unit IIb (~14.2-12.9 ka), which we suggest reflects Mono Lake at lowstand.

5.3 Unit III (~12.9-10.9 ka)

The age model for Unit III is constrained by two pollen ^{14}C dates and one plant macrophyte ^{14}C date. The two horizons dated by pollen are located at 653 and 503 cm in the composite UWI15 stratigraphy, whereas the horizon containing the dated macrophyte is located at 497 cm (Table 1). The pollen sample at 653cm was dated to 14.9 ka. The pollen sample at 503 cm was dated to 11.7 ka, while the plant macrophyte at 497 cm had a date of 12.9 ka. This reversal could be the result of reworking of older lake deposits via riverine incision during a lake level changes, a process which has been described from other large lakes (Meyers and Lallier-Verges, 1999; McFadden et al., 2004).

The paleo-shoreline analysis conducted by Ali (2018) showed that Mono Lake achieved a highstand ~13.0-12.0 ka at the onset of the Younger-Dryas (Y-D) (~12.9-11.7ka) (Figure 2). Ali (2018) explains that a potential control on Mono Lake hydrology is sea surface temperatures in the North Atlantic. Following this interpretation, wintertime precipitation in the Sierras is enhanced by a strong subtropical jet, which is caused by the migration of the Intertropical Convergence Zone (ITCZ) to the south; ITCZ movement is in response to surface pressure anomalies in the North Atlantic that co-occur with large extents of sea ice (Chiang et al., 2014; Cvijanovic et al., 2017). In

contrast to the interpretations of Ali (2018), some other researchers have described the Y-D as a cool and dry interval in the Sierras (Benson et al., 1997; Mensing, 2001; MacDonald et al., 2008). According to MacDonald et al. (2008), chrionomid-based lake-water temperature reconstructions indicate that Starkweather and Barrett Lakes were ~2-4°C cooler during the Y-D; these basins are ~37 and 45 km from Mono Lake, respectively. If water temperatures at Mono Lake were similarly low, the decreased evaporation may have been a positive feedback that helped facilitate transgression, in addition to higher precipitation arising from a southerly displaced ITCZ. Our chemostratigraphic and physical properties data (Figure 8) provide evidence in support of higher Mono Lake levels during Unit III.

Lower Unit III deposits encompass the Y-D highstand, whereas the upper portion of Unit III appears to reflect deposition during a regression. Basal Unit III muds (~655-591 cm; ~12.9-12.2 ka), preserve fine laminations, which is consistent with an anoxic or strongly dysoxic lake floor that inhibits the activity of bioturbating benthos (Meyers, 2003). Moving upsection, the muds are laminated and change to olive green and red colors with diffuse contacts; thin, normally graded grey sandy beds are also occasionally present (Figure 9). We interpret this sedimentological transition to mark the inception of regression and a deeper position of the redox front within the sediment column, allowing at least periodic oxidation and reworking of the muds on the lake floor by bioturbation (Potter et al., 2005). Similarly, Newton (1994) and Zimmerman et al. (in rev.) have suggested that the loss of fine laminations in Mono Lake sediments are indicative of lake mixing or lake level decline. The upward fining sand beds are interpreted as Bouma sequence-style Ta beds, deposited by decelerating turbidity currents (Middleton and

Hampton, 1973). We suggest that as water levels fell near the conclusion of the Y-D (~11.7 ka), Mono Lake margins and delta fronts became unstable, leading to mass wasting and downslope transport of sediment. At 498cm (~11.2 ka), Unit III sediments transition again to diffusely laminated light grey muds, which persist until the upper contact.

Unit III is characterized by uniformly low MS, with the exception of sandy Ta beds, which produces high values (Figure 8). Low MS values for the muddy strata point to minimal transport of terrigenous magnetic grains to the core site early in Unit III time, which is consistent with high lakes levels, back-stepping deltas, and sparing potential for dilution influencing organic facies development during the Y-D. The TOC concentrations during the Y-D were 0.4-3.9 wt. % (mean = 2.1 wt. %), and as a result, we interpret that Mono Lake was most likely eutrophic during this time. Evidence in support of this interpretation comes from relatively enriched $\delta^{13}C_{ORG}$ values and high BiSi (mean = 13.0 wt. %) concentrations; Cohen (2003) notes that it is common for the algal composition of eutrophic lakes to be dominated by diatoms. Furthermore, we interpret that Mono Lake was not nutrient limited, as the $\delta^{15}N_{ORG}$ values remain low (mean = 6.0‰), which may have resulted from seasonal water column mixing (e.g., Talbot and Johannessen, 1992; Cohen, 2003).

Unit III has highly variable BiSi and TIC throughout the section; TIC increases abruptly above the Unit II-III contact and has a mean concentration of ~1.2 wt. % (Figure 9). Benson et al. (2002) argued that for many Great Basin lakes, an inverse relationship exists between lake level and TIC concentrations. However, higher concentrations (mean = 1.4 wt. %) of TIC from ~12.9-12.2 ka, during the Y-D highstand, are more consistent

with the mechanism of enhanced Ca^{2+}-rich runoff to Mono Lake as water levels rose, allowing authigenic carbonate to precipitate from the water column. Yet the carbonate content of Unit III is vertically variable. Moving upsetion, smear slide analysis of upper Unit III revealed the presence of ostracodes, which suggests that shallow water carbonates were being reworked and transported into deeper water, consistent with falling water levels following the Y-D highstand. The TOC and $\delta^{15}N_{ORG}$ are relatively low from ~12.9-11.7 ka, but these indicators change from ~11.7-10.9 ka and are marked by high amplitude variability. In contrast, gradual trends in $C:N_{ATM}$ and $\delta^{13}C_{ORG}$ toward higher values approaching the upper contact characterize Unit III (Figure 8).

The chemostratigraphy of Unit III shows that the Mono Lake ecosystem responded to the Y-D highstand and the regression that followed. For example, there is a prominent $\delta^{15}N_{ORG}$ shift (over a range of ~4.0‰) towards higher values at ~11.7 ka. At the base of Unit III, $\delta^{15}N_{ORG}$ values are relatively low (mean = ~6.0‰) with minor variability, whereas at ~11.7 ka, $\delta^{15}N_{ORG}$ increases and becomes highly variable, reaching values >10.0‰ (Figure 8). This enrichment in $\delta^{15}N_{ORG}$, coupled with gradually increasing $C:N_{ATM}$ (mean = 15) towards the Unit III-IV boundary, suggests that Mono Lake was experiencing an increase in terrestrial organic-matter delivery (Figure 11), perhaps associated with margin collapse or from down-cutting streams and lowstand delta development as lake levels declined. In addition to enriched $\delta^{15}N_{ORG}$ and high relative $C:N_{ATM}$, very high TOC values (≤ 9 wt. %) mark sediments ~11.7-10.9 ka. We interpret these data to reflect offshore focusing of organic matter as lake-level fell, which is a process that has been invoked to explain Mono Lake TOC concentrations in the historic period (Tenzer et al., 1997; Meyers and Lallier-Verges 1999).

Following this model, wave-enhanced resuspension of organic matter is moved offshore as water levels and wave base fall; the presence of ostracode valves in these deposits suggest this mechanism is viable, as wave reworking of the littoral zone could transport the low density bioclasts offshore. Alternatively, falling lake levels may have increased salinity, which could inhibit microbial respiration or increase the strength of water column stratification, leading to higher TOC through enhanced organic matter preservation (Meyers and Teranes, 2001). However, the diffuse red and olive green laminations of the regressive phase argue against stronger water column stratification and lake-floor anoxia at this time, and thus we favor offshore focusing of nearshore organic matter as the dominant mechanism of organic enrichment.

5.4 Unit IV (~10.9-8.7 ka)

The age model for Unit IV consists of five ^{14}C dates on plant macrophytes. Moving from the base to the top of the unit, the dates are: 10.6 ka at 460cm, 11.6 ka at 424cm, 11.5 ka at 422cm, 11.6 ka at 421cm, and 9.7 ka at 368cm (Table 1). There are two instances within Unit IV where ^{14}C dates are out of stratigraphic order, but the error bars for the reversed ages overlap the adjacent dated horizon (Figure 10). The explanation for the reversed ages is presently unknown, but small sample sizes or organic material that was temporarily stored on the landscape and became reworked by physical processes could be responsible.

Unit IV consists of finely laminated to thinly bedded muds and silts; the relative grain size of these deposits are the finest in the UWI15 core. Sands are rare in Unit IV and where they do exist, beds are thin and exhibit normal grading. Unit IV has relatively low MS, except for the thin sandy beds near the basal contact. The MS response of the

sandy beds is symmetrical, in contrast with the asymmetric MS response pattern of turbidites at lower stratal levels in the UWI15 core, as well as turbidites reported on from other lakes in the region (Osleger et al., 2008; Noble et al., 2016). This MS response has been documented for turbidites formed from remobilization of hemipelagic sediments on sub-lacustrine slopes (Moernaut et al., 2014). Such turbidites usually have a thin sandy base, a thicker homogenous silty/diatomaceous mid-layer, and a thin capping clay layer (Figure 12). Comparatively, lacustrine turbidites with asymmetric MS are usually comprised of siliciclastic detritus, and form from delta collapse, river floods, and onshore landslides that propagate into the basin (Moernaut et al., 2014; Van Daele et al., 2015) (Figure 12). The sedimentology and MS response of Unit IV turbidites are most consistent with an origin linked to remobilized subaqueous slope material. We interpret that minor changes in lake level during Unit IV time may have been responsible for initiating these sub-lacustrine gravity flows.

Most of the geochemical indicators in Unit IV undergo gradual changes, suggestive of a slow but important environmental transition following the post Y-D regression at Mono Lake. For example, BiSi concentrations and $C:N_{ATM}$ values decrease gradually from ~15.0 to 5.0 wt % and ~17 to 13 towards the upper contact, respectively (Figure 8). Similarly, $\delta^{13}C_{ORG}$ undergoes a gradual 2.0‰ shift towards more positive values moving upsection. TOC (mean = 2.0 wt. %) and $\delta^{15}N_{ORG}$ (mean = 5.0‰) show small changes only from the basal to the upper contact (Figure 8). We interpret that the $\delta^{15}N_{ORG}$, $C:N_{ATM}$, and $\delta^{13}C_{ORG}$ chemostratigraphy as evidence of a gradual change in organic matter provenance, from mixed terrestrial and aquatic material to one dominated by lacustrine algal sources.

The high and largely invariant TOC concentrations and low MS values suggest that the lake was not experiencing terrigenous dilution of organic matter, and it is unlikely that turbidity constrained light penetration or the width of the photic zone, as may have been the case in the late Pleistocene. Rather, we interpret that Mono Lake experienced a relatively high rate of primary productivity and perhaps enhanced organic matter preservation ~10.9-8.7 ka. The $\delta^{13}C_{ORG}$ chemostratigraphy supports a eutrophic Mono Lake during Unit IV time. Enrichment of sedimentary $\delta^{13}C_{ORG}$ occurs as ^{12}C is depleted from the water column, which can be accomplished by high rates of algal productivity selectively taking up the light isotope during photosynthesis (Cohen, 2003).

The sharp laminations of Unit IV are consistent with an absence of bioturbation at the core site, which may have been enhanced by lake bottom anoxia. Likewise, the fine particle sizes of these deposits may have limited oxidants in pore spaces, which may have further enhanced organic matter preservation (Meyers, 2003; McGlue et al., 2012). This interpretation is supported by insights from Newton (1994), who suggested that starting around ~10 ka, Mono Lake was likely meromictic with a salinity close to that of seawater. Meromictic lakes have actively mixing epilimnions, whereas the deeper hypolimnion is sequestered below a pycnocline defined by O_2 levels, temperature, or salinity. It is not unusual for meromictic lakes to preserve considerable organic matter, due to low oxygen levels at the sediment water interface that limit bioturbation and microbial respiration (Talbot and Livingstone, 1989; Newton, 1994; Meyers, 2003).

However, meromictic lakes may be nutrient limited, as internal cycling of nitrogen and phosphorus is limited by a lack of water-column turnover. The TOC concentrations, $C:N_{ATM}$, and $\delta^{13}C_{ORG}$ data all point towards high algal productivity at

Mono Lake during Unit IV time; if the lake was meromictic, it was not severely nutrient limited. However, BiSi concentrations vary over 8.0 wt. % in the unit, and are considerably lower than Unit III for both highstand and lowstand conditions. Smear slides from Unit IV muds show diatoms as a common component, but amorphous organic matter is prominent, which we interpret as evidence for Mono Lake being conducive habitat for diverse algae types. These observations suggest that diatoms may have been out competed for resources by other phytoplankton relative to the Y-D highstand. This may have resulted from increased water column stability associated with meromixis, which favors nitrogen-fixers as recirculation of DIN is limited by the presence of a chemocline, as evident by the mean $\delta^{15}N_{ORG}$ ~5.0‰ (e.g., Talbot and Johannessen, 1992).

Unit IV was deposited during a period that has been described as cool and wet for the Great Basin, and some of our data are consistent with this paleoenvironmental interpretation (Noble et al., 2016; Zimmerman et al., in rev.). From a process perspective, our $C:N_{ATM}$ data are consistent with the findings of Noble et al. (2016), who suggested that during cool intervals, transport of terrestrial organic matter to lakes is limited by snow cover in the watershed, which restricts the type and distribution of land plants, and shorter periods of snow melt, which reduces runoff in the spring and summer seasons. However, the recent paleo-shoreline reconstruction provided by Ali (2018) shows that water levels at Mono Lake were fluctuating in the early Holocene, with lake surface elevations considerably lower than the two prominent lake level highstands centered on ~16 ka and ~13-12 ka.

Moderate carbonate concentrations (mean TIC =1.0 wt. %) in Unit IV suggest that Mono Lake was more dilute in the early Holocene than it is in the present day, though

mechanisms of carbonate formation may not be analogous given the alkalinity of the modern system and potential for microbial mediation of carbonate sedimentation (e.g., Brasier et al., 2018) (Figure 8). This pattern of low early Holocene carbonate concentrations is also true for a long sediment core (BINGO10/4A) collected from shallow water in Mono Lake, which was interpreted to have resulted from a relatively wet paleoclimate (Zimmerman et al., in rev.). Moderate TIC concentrations in the UWI15 core ~10.9-8.7 ka is consistent with a relatively deep lake, assuming hydroclimate alone is responsible for $CaCO_3$ precipitation at the core site. The available paleo-shoreline data from ~10.9-8.7 ka suggests that lake level oscillated between ~1975 and ~1955 m.a.s.l., however the full extent of these changes are still not completely known (Ali, personal communication, 2018).

Since our core was collected from a relatively deep location in Mono Lake (18 m water depth), minor changes in lake level are not likely to impart large changes in deepwater sedimentology or geochemistry. For example, turbidites, which appear to be generated around regression events in the Mono Basin, are found in the base and middle of Unit IV, but their sedimentology suggests an origin linked to the remobilized hemipelagic sediment, rather than prolonged episodes of incision associated with high amplitude lowstands (Figure 12). Further, Unit IV contains some of the finest and most distinct laminae in the entire core. Preservation of fine laminations is most consistent with a relatively deep lake with anoxic bottom waters. Therefore, our data suggest that lake level oscillations between ~1975-1955 m.a.s.l. during Unit IV time did not have a strong impact on sedimentology or organic facies development in deepwater Mono Lake,

though the same may not have been true in littoral and supralittoral environments examined by Ali (2018).

5.5 Unit V (Va ~8.7-6.3 ka; Vb ~6.3-4.2 ka)

The geochronology for Unit V is constrained by 10 ^{14}C dates within the depth range of ~354-296 cm. The dates consist of plant macrofossils (*n=6*), purified pollen (*n=2*), and charcoal (*n=1*) (Table 1). At the base of the unit, there are two pollen dates at 354 and 353 cm, with ages of 9.1 ka and 9.2 ka. The oldest date in the unit is a charcoal sample located at 337 cm, which yielded a date of 9.9 ka, suggesting that the charcoal may have been reworked for several centuries on the landscape prior to deposition. The uppermost part of Unit V (~220-235 cm) contains three tephras, which have been correlated (using MS and Ca/Ti peaks; Zimmerman, personal communication, 2018) to three tephras identified and dated using ^{14}C in the shallow-water BINGO 10/4A core (Zimmerman et al., in rev.). The ages for the three tephra beds are ~4700, 5100, and 5400 cal yr BP. These tephras and their associated ^{14}C ages suggests that our ^{14}C dated horizon at 296 cm (6.5 ka) is a reliable upper constraint on the unit's chronology (Table 1).

Unit V consists of laminated medium brown muds and occasional silts (Figure 9). The laminae contacts vary from diffuse to sharp. Notably, the MS response for Unit V is low, except for the three tephra-associated peaks near the upper unit contact (Zimmerman et al., in rev.) (Figure 8). The $\delta^{13}C_{ORG}$ and $\delta^{15}N_{ORG}$ values remain relatively enriched and only shift ~4.0‰ for the entire unit. $C:N_{ATM}$ values remain consistent and only vary by ~4.0 aside from an outlier at the base of the unit, which we interpret to be anomalously low due its proximity to a tephra. Concentrations of TIC are marked by high amplitude variability (~5.0 wt. %) near the base of Unit V, but variability and maximum values

decline upsection (~2.0 wt. %). BiSi concentrations remain relatively low for the entire unit (mean = 8.0 wt. %), with values decreasing towards the Unit VI boundary. Comparatively, TOC concentrations show a gradual ~2.0 wt. % increase towards the Unit VI boundary. The muds in Unit V are dominantly composed of hemipelagic material, as evident by the low MS values, which suggests detrital influx was not an important factor in the development of organic facies during Unit V time.

Much of Unit V time (~8.7-4.2 ka) overlaps with the Holocene Hypsithermal (~9.4-5.3 ka), an interval which many studies from the eastern Sierra Nevada interpret as relatively dry (Davis, 1999; Osleger et al., 2008; Zimmerman et al., in rev.). Importantly, paleo-shoreline data from Mono Lake are unavailable for this period. During the Holocene Hypsithermal, numerous Great Basin lakes were at lowstand, including Owens and Pyramid Lakes (Benson et al., 1997; Mensing et al., 2004). Furthermore, palynological studies from the region identified evidence for early Holocene aridity. For example, the Mono Lake pollen study by Davis (1999) noted a ~5% increase in halophytic Chenopodiaceae-*Amaranthus* and *Sarcobatus* pollen between 9000-5000 ^{14}C yr B.P., which suggested drought and salinity tolerant flora around Mono Lake. A drying trend in Mono Lake was recorded in the BINGO10/4A shallow water core from ~7.9-4.8 ka, based on the presence of shallow water, high energy carbonate facies, indicative of close proximity of the coring site to the shoreline (Zimmerman et al., in rev.).

We interpret the elemental and isotopic data to reflect a relative lake level lowstand during Unit Va (~8.7-6.3 ka). Conditions of low water level elevation are most clearly expressed in the spiky TIC chemostratigraphy (Figure 8). Prominent peaks in the TIC curve are generated in Unit Va due to ostracodes and sand-sized grains of tufa,

which form bleb-shaped yellow-white laminae observed on thin sections. These sedimentological features share a number of similarities to the shallow water aragonite "flake mud" described by Newton (1994). In Mono Lake, algal tufa forms in the photic zone at depths ≤ 5m (Ali, 2018). The presence of tufa-derived carbonate in Unit Va laminations suggests that: (a) the UWI15 core site was within the photic zone or at the shoreline, or (b) shallow water carbonates were reworked by waves and transported offshore, ultimately accumulating in deepwater. The fine laminations of Unit Va muds argues against deposition in the littoral or supralittoral zones, and therefore we favor reworking of exposed littoral shelves during a regression as the best explanation for the TIC chemostratigraphy.

Notably, much of Unit Va occurs during a peak in late summer Northern Hemisphere insolation, and the initiation of the North American monsoon is believed to have occurred around 8.0 ka (Barron et al., 2012). It is plausible that periodic summer rainstorms may have influenced wave action and reworking of Mono Lake's littoral zone during Unit Va, leading to offshore transport of both inorganic and organic carbon. By analogy, Godsey et al. (2011) interpreted that storms were important agents for reworking nearshore carbonates into offshore environments during a regressive phase of Lake Bonneville. Today, the North Pacific High shifts to the north during the summer, which restricts rainstorms to higher latitudes, while a northerly ITCZ induces summer monsoon conditions (Zimmerman et al., in rev.).

The geochemistry of Unit Va consists of low BiSi concentrations (mean = 8.0 wt. %), moderate TOC concentrations (mean = 2.0 wt. %), and relatively enriched $\delta^{15}N_{ORG}$ and $\delta^{13}C_{ORG}$ (means of ~6.0‰ and -22.0‰, respectively). We interpret that offshore

focusing of macrophyte-rich organic matter by waves likely accompanied the transport of nearshore carbonates to the UWI15 site. This is also in clear evidence from the number of plant macrophyte fragments available for ^{14}C dating. The $C:N_{ATM}$ values remain relatively stable throughout Unit V and average ~14, suggesting a mixture of lacustrine and terrestrial flora to the organic matter pool. We interpret that the TOC concentrations, as well $\delta^{15}N_{ORG}$ and $\delta^{13}C_{ORG}$, reflect contributions of macrophyte and terrestrial organic matter to Unit Va. A cross-plot of $\delta^{13}C_{ORG}$ with $C:N_{ATM}$ (Figure 11) suggests the presence of C_4 plant matter in Unit Va (~8.7-6.3 ka) (Meyers, 2003). Because C_4 plants are adapted to arid or water stressed environments, these data are in accord with a low lake level interpretation for Mono Lake at this time, as well as the palynological observations of Davis (1999). Moreover, warmer water cannot dissolve as much CO_2 as cooler water. Talbot and Johannessen (1992) suggested that in endorheic lakes, warming of lake surface waters may increase the volatilization of ammonia, which drives the isotopic enrichment of ^{13}C and ^{15}N in organic matter.

The sediments of Unit Vb are a dark yellow-brown with intermittent diffuse and sharp laminae contacts (Figure 9). The geochemistry of Unit Vb suggests only minor changes in paleolimnology and organic facies development from ~6.3-4.2 ka. During this time, wet intervals have been identified in numerous lakes in the region from ~6.3-3.0 ka, based on turbidites, pollen, algae, and charcoal proxies (Mensing et al., 2004; Osleger et al., 2008; Noble et al., 2016). In our data, the clearest evidence of an environmental change comes from the relatively invariant TIC values, suggesting that wave reworking of nearshore carbonate declined in this interval. The absence of reworked nearshore

carbonates suggests that convective rainstorms were probably not an important control on wave action and offshore sediment focusing at this time.

Beginning ~6 ka, a decrease in Northern Hemisphere summer insolation caused summer temperatures to decline (COHMAP, 1988). If we assume a decline in summer temperatures at Mono Lake, an increase in dissolved CO_2 due to a cooler surface waters may be a viable explanation for the trend toward more negative $\delta^{13}C_{ORG}$ values observed in Unit Vb (Talbot and Johannessen, 1992; Cohen, 2003; Noble et al., 2016). A crossplot of $\delta^{13}C_{ORG}$ with $C:N_{ATM}$ shows a slight change in organic matter provenance, favoring C_3 vegetation for this unit (Figure 11). Unit Vb data overlap organic geochemical values from Unit IV, a known interval when the Sierra Nevada were cooler and wetter (Noble et al., 2016; Zimmerman et al., in rev.). $C:N_{ATM}$ values for Unit Vb remain stable relative to the underlying deposits, however $\delta^{15}N_{ORG}$ declines towards the Unit VI boundary, suggesting a slight increase in productivity compared to Unit Va.

This decreasing trend in $\delta^{15}N_{ORG}$, coupled with a decreasing trend in BiSi, possibly indicate an increase in water column stability and limited recirculation of DIN suggesting diatoms may have been in competition with other phytoplankton for nutrient resources (e.g., Cohen, 2003; Talbot and Johannessen 1992). TOC concentrations for Unit Vb is ~1.0 wt. % higher than the TOC concentrations for Unit Va, suggesting preservation was slightly higher and that Mono Lake was likely meromictic.

5.6 Unit VI (4.2-0.3 ka; gap from 4.2-1.1 ka)

The geochronology for Unit VI is constrained by one ^{14}C date on a plant macrophyte below the coarse pumice tephra and two ^{14}C dates above the pumice tephra on a plant macrophyte and an insect carapace (Table 1). The lowermost ^{14}C date comes

from material recovered at ~205 cm, which produced a date of 4.2 ka. The dates made on the macrophyte and insect parts were recovered from the same horizon at ~96 cm and yielded ages of 1.1 ka. The chronology of Unit VI is also informed by the presence of a 0.5 cm thick white sandy layer containing volcanic glass at 66 cm, which we interpret to be a candidate for the North Mono tephra (NMT), a well-studied eruptive deposit in the Mono Basin that formed ~625 cal yr BP. Directly overlying the NMT, there is ~1.0 cm thick package of laminated mud, which is in turn overlain by a ~2.0 cm thick package of grey mud composed of diatoms and volcanic glass. The grey layer shares some characteristics with sediments associated with the Paoha Island uplift, which occurred ~250 cal yr BP (Stine, 1987; Newton, 1994; Benson, 2003; Colman et al., 2014).

Unit VI is characterized by a massive grey pumice gravel tephra (~80 cm) bounded on top and bottom by massive sandy muds (Figure 9). The basal sediments are ~30 cm of massive, distorted dark brown sandy mud that coarsens upward into gravel and pebble-sized tephra fragments; these sediments produce high MS peaks. The top of the unit is characterized by ~30 cm of massive grey-brown sandy mud with relatively intact bedding. Our geochemical sampling focused on the muddy sands that sandwich the massive tephra.

We interpret the sandy mud and gravel pumice tephra to be a debris flow deposit. The presence of heavily disturbed bedding in the basal sandy mud and the weak inverse grading of the overlying tephra deposit suggest that a debris flow origin is possible (Middleton and Hampton, 1973). The flow that transported this material eroded the lake floor, resulting in the time gap within the record.

The origin of the pumice is not entirely known and its spatial extent is unclear. The CHIRP seismic survey completed by Colman et al. (2014) did not produce clear evidence for a deposit of this kind. A similar pumice layer is not present at the shallow water BINGO10/4A core site, which is ~ 1.8 km from the UWI15 site (Zimmerman et al., in rev.). As a result, we tentatively interpret this deposit as a sub-lacustrine debris flow that eroded away ~4000 yrs of late Holocene section. One hypothesis on the source of this massive pumice relates to the sub-lacustrine Java Islet eruption ~1670 cal yr B.P., when the lake surface was believed to lie at ~1948 m.a.s.l.

The Java Islet eruption is known for voluminous pumice ejecta, which floated to the surface of the lake and drifted on currents until they became waterlogged and sank (Stine, 1990). The majority of the Java Islet pumice has been found in the western half of Mono Lake (Stine, 1990), which is consistent with its emplacement in the western embayment. Following this hypothesis, pumice blocks sank to the lake floor near the western embayment shoreline once they became waterlogged, and they were dislodged by an earthquake or volcanic eruption and drove a downslope movement such as a slide or semi-cohesive debris flow. The inception of the gravity flow certainly followed the Java Islet eruption, given the time needed to transport the pumice and for it to become waterlogged.

However, the mechanism responsible for remobilizing the large chunks of pumice and moving them downslope to the UWI15 core site remains uncertain. One plausible candidate is an earthquake or series of earthquakes associated with a volcanic eruption, such as the South Mono eruption (~1350 cal yr BP). Mono basin is seismically active, and previous research by Bursik et al. (2003) showed that volcanic events are frequently

accompanied by one or more large earthquakes (e.g., the North Mono eruption ~625 cal yr BP). Bursik et al. (2014) noted that the South Mono eruption was one of the largest in the southwest US during the Holocene, and it is plausible that large earthquakes preceded or followed the eruption that destabilized the lake margin and shunted Java Islet pumice blocks in a debris flow to the core site. Interestingly, the dated organic materials that overlie the debris flow deposit range from 970-1260 cal yr BP (inclusive of 2-sigma error) (Table 1), which postdates the South Mono eruption. The South Mono tephra is not clearly expressed in the overlying sandy mud, but most of the coarse grains in that deposit are indeed tephra.

The top of the unit is characterized by light greyish brown sandy mud with relatively low BiSi (mean = 5.0 wt. %), low-moderate TIC (mean = 0.5 wt. %) and TOC (mean = 1.0 wt. %), and moderate $C:N_{ATM}$ (mean = 13). These values tend to increase towards the Unit VII boundary which suggests that immediately following the emplacement of the pumice, the lake floor was unstable. As the core site slowly stabilized and hemipelagic sedimentation resumed, all of the indicators increased more or less synchronously, possibly indicating a return to background lacustrine sedimentation. The $\delta^{15}N_{ORG}$ and $\delta^{13}C_{ORG}$ values are variable and display ~3.0‰ shifts towards more depleted values approaching the upper contact, and higher BiSi concentrations indicate an increase in diatom productivity. This is coupled with low-moderate TIC concentrations, which indicate that rivers were supplying Ca^{2+} ions to the lake at this time. The $C:N_{ATM}$ chemostratigraphy indicates that terrestrial sources contributed organic matter to the lake at this time.

5.7 Unit VII (~250yrs-present)

The geochronology for Unit VII is unconstrained by ^{14}C dates. However, this unit directly overlies the Paoha Island mudflow deposit as identified by Zimmerman (personal communication, 2016). Therefore, we have interpreted this unit is the last ~250 years of sedimentation in Mono Lake. With this constraint on the basal age of Unit VII, our sampling resolution (~4cm) provides multi-decadal resolution (~17 yrs between samples).

Unit VII consists of ~60 cm of finely laminated muds, which range from dark brown at the top of the unit to greyish green at the base (Figure 9). This unit is characterized by high TIC (mean = 3.0 wt. %) and TOC (mean = 5.0 wt. %) concentrations with low MS, BiSi, and $C:N_{ATM}$ values (Figure 8). The isotope data for this unit are the most enriched for the entire core, with $\delta^{13}C_{ORG}$ and $\delta^{15}N_{ORG}$ values averaging ~ -21.0‰ and 13.0‰, respectively. The low MS data coupled with high TOC concentrations suggest that the lake was productive (eutrophic) and terrigenous dilution did not play a major role affecting organic enrichment.

Furthermore, when interpreted in concert with the enriched $\delta^{13}C_{ORG}$ and $\delta^{15}N_{ORG}$, the chemostratigraphic data suggests Mono Lake experienced high rates of productivity as both the DIC and DIN pools were being drawn down during this time. The low $C:N_{ATM}$ values (mean = 10), suggests the dominant organic matter source for the lake during this time is lacustrine algae, but the flora was not dominated by diatoms as BiSi concentrations show a marked decline towards the top of the unit. However, smear slide observations have confirmed the presence of green algae, which suggests that the diatoms were being out competed during this time. Not only was Mono Lake highly productive

during the last ~250 yrs, it was also experiencing increased preservation and bottom water anoxia, as evident by the preservation of fine laminations and lack of sedimentary features consistent with bioturbation.

During the deposition of Unit VII, the lake experienced some significant changes in the water chemistry due to water diversions to the Los Angeles Aqueduct beginning in the 1940s. These water diversions caused Mono Lake shoreline elevation to drop ~14 m and forced lake water salinity and alkalinity to double due to evaporative concentration (Stine, 1990; Newton, 1994; Jellison et al., 1996).

Today, Mono Lake is a warm monomictic lake that is stratified via a thermocline. The lake mixes annually when surface cooling and wind shear break down the thermal stratification allowing for nutrient cycling in the winter that impacts the food web and productivity (Oremland et al., 1987; MacIntyre et al., 1999). However, through the work of Jellison and Melack (1993), it is clear that water-column stratification in Mono Lake is readily affected by climatic variations. For example, an influx of freshwater led to the onset of meromixis, which occurred following heavy rainfall related to the 1982-1983 ENSO event. Establishing meromixis in Mono Lake may lead to denitrification and thus, more positive sedimentary $\delta^{15}N_{ORG}$ values (Cohen, 2003). This is a common trend in lakes that transition from a seasonal-mixing regime to a permanent/strongly stratified lake as the volume of the lake's hypolimnion changes (e.g., Hecky et al., 1996).

Furthermore, as the lake-water pH increases (modern pH at Mono Lake ~10), so does the volatilization of ammonia, which causes a strong enrichment in $\delta^{15}N_{ORG}$ values. This is most commonly seen in closed-basin lakes under highly evaporative conditions and can be used as an indirect indicator for increased aridity (Cohen, 2003). Thus, this

change in water chemistry and mixing regimes should be taken into account when interpreting the $\delta^{13}C_{ORG}$ and $\delta^{15}N_{ORG}$ values for Unit VII.

Table 3: Results of the chemostratigraphic analysis for each sample of UWI15. (TN = total nitrogen)

Depth (cm)	$\delta^{13}C_{ORG}$ (‰ VPDB)	$\delta^{15}N_{ORG}$ (‰ Air)	C:N (atomic)	TIC (wt. %)	TOC (wt. %)	BiSi (wt. %)	TN (wt. %)
0	-27.00	11.39	9	3.09	7.59	6	1.04
4	-21.91	10.82	8	2.28	4.87	7	0.71
8	-25.51	11.50	9	1.95	6.20	8	0.80
12	-20.07	10.56	8	2.87	4.60	6	0.71
16	-19.68	11.00	10	2.67	4.88	6	0.59
20	-19.44	11.02	10	2.32	4.96	7	0.61
24	-18.99	9.92	8	2.86	5.55	6	0.79
28	-19.89	9.55	11	2.33	6.55	8	0.73
32	-19.04	11.11	11	2.71	6.01	8	0.66
36	-18.52	13.56	10	3.07	3.92	8	0.48
40	-17.96	13.95	11	2.58	5.02	11	0.55
44	-17.54	16.88	12	2.67	5.34	12	0.01
48	-18.09	18.79	10	2.83	4.21	9	0.51
52	-19.78	18.33	13	2.34	4.38	15	0.41
56	-20.13	18.63	11	2.37	3.74	15	0.39
60	-24.85	14.45	10	2.20	3.25	27	0.40
64	-23.95	8.03	18	0.88	1.80	8	0.11
68	-21.04	11.76	17	0.86	1.19	7	0.08
70	-21.07	11.29	13	0.85	0.91	6	0.08
72	-22.49	10.17	18	0.73	1.11	7	0.07
76	-22.39	11.55	16	0.69	0.76	5	0.06
80	-21.17	13.11	15	0.60	0.64	4	0.05
82	-21.09	12.83	13	0.55	0.39	3	0.04
84	-20.64	12.65	10	0.51	0.34	4	0.04
88	-22.20	10.82	8	0.52	0.36	4	0.05
92	-20.01	9.57	6	0.25	0.18	3	0.03
94	-20.53	9.87	12	0.77	0.62	5	0.06
187.55	-22.23	9.01	11	2.23	1.05	5	0.11
192	-22.22	8.77	18	2.23	2.40	8	0.15
196	-22.20	15.86	3	1.71	1.74	5	0.62
199.55	-22.63	8.83	18	2.62	1.66	6	0.11
204	-23.09	5.71	13	1.72	3.67	11	0.32
208	-23.84	6.25	15	1.63	4.35	15	0.34
211.55	-23.79	6.28	15	1.52	4.42	7	0.35
216	-21.68	7.28	15	1.80	2.89	8	0.23
220	-22.31	7.37	16	0.34	0.98	4	0.07
223.55	-22.69	4.94	15	1.16	4.18	8	0.32
228	-23.80	6.94	15	0.13	0.19	3	0.01
232	-22.73	5.29	15	0.22	0.35	5	0.03
235.55	-23.60	4.53	16	1.04	4.14	7	0.31

Table 3: (Continued)

Depth (cm)	$\delta^{13}C_{ORG}$ (‰ VPDB)	$\delta^{15}N_{ORG}$ (‰ Air)	C:N (atomic)	TIC (wt. %)	TOC (wt. %)	BiSi (wt. %)	TN (wt. %)
240	-23.69	4.64	14	1.36	3.97	6	0.32
244	-22.29	3.48	14	1.22	3.73	8	0.31
247.55	-22.79	5.69	14	1.10	2.42	6	0.20
252	-21.78	4.83	14	0.99	4.18	9	0.35
256	-22.84	5.66	14	1.32	3.14	7	0.27
259.5	-23.26	5.85	15	1.08	3.23	6	0.25
264	-23.94	6.17	14	1.33	3.89	11	0.32
268	-21.29	5.49	14	1.28	3.39	7	0.28
271.5	-22.14	6.61	16	1.50	3.21	9	0.24
276	-20.70	7.23	13	1.56	3.04	11	0.27
280	-21.54	7.20	13	1.17	3.57	7	0.32
283.5	-21.62	6.47	14	1.32	3.20	9	0.27
288	-20.58	8.11	14	1.44	2.54	8	0.21
292	-21.25	6.42	13	2.26	1.99	8	0.18
295.5	-21.76	6.99	15	4.86	1.97	7	0.16
300	-20.92	6.43	13	1.29	2.66	9	0.23
304	-22.20	6.45	14	1.70	2.24	8	0.19
307.5	-21.68	5.79	14	1.42	2.34	8	0.20
312	-21.66	5.64	16	0.94	1.90	7	0.14
316	-20.28	6.64	15	1.13	2.52	6	0.20
319.5	-20.52	6.39	15	3.02	2.59	6	0.20
324	-22.29	5.15	15	1.75	2.24	6	0.18
328	-22.90	5.83	15	1.61	2.12	10	0.17
331.9	-23.86	5.38	15	1.76	2.49	9	0.19
336	-22.33	4.30	15	1.21	1.81	10	0.14
340	-22.23	5.57	3	2.95	0.49	9	0.17
343.9	-22.00	5.66	16	0.38	0.47	3	0.03
348	-21.63	5.95	12	2.40	2.31	8	0.22
352	-22.49	3.97	12	1.16	3.22	11	0.31
355.9	-22.88	5.51	13	1.41	2.44	5	0.22
364	-22.94	6.16	12	1.02	2.27	7	0.21
367.4	-23.70	5.86	14	1.29	2.66	8	0.22
372	-22.83	5.35	12	0.94	2.66	6	0.26
376	-23.16	5.37	13	1.02	2.55	8	0.22
380.3	-23.61	6.08	14	1.17	2.51	8	0.20
384	-23.59	5.47	13	1.17	2.90	10	0.26
388	-23.81	5.64	14	0.93	2.20	8	0.19
392.8	-23.95	3.47	14	1.02	2.56	7	0.22
396	-23.10	3.15	13	1.12	2.31	8	0.21
400	-24.13	4.46	14	0.79	2.46	6	0.20

Table 3: (Continued)

Depth (cm)	$\delta^{13}C_{ORG}$ (‰ VPDB)	$\delta^{15}N_{ORG}$ (‰ Air)	C:N (atomic)	TIC (wt. %)	TOC (wt. %)	BiSi (wt. %)	TN (wt. %)
403.8	-23.84	5.04	15	0.93	2.15	8	0.17
408	-24.20	4.97	14	0.93	2.58	10	0.21
412	-23.90	4.22	14	0.76	2.25	8	0.19
415.8	-24.30	5.04	15	0.87	1.99	8	0.15
420	-23.52	5.08	14	0.63	1.88	8	0.16
424	-23.84	4.09	14	0.77	2.10	9	0.18
427.8	-23.95	4.24	15	0.94	2.53	9	0.20
432	-23.59	5.35	15	1.14	1.36	7	0.10
436	-25.13	3.77	15	0.94	2.46	10	0.19
439.8	-25.20	4.55	17	0.84	1.28	7	0.09
444	-23.20	4.22	15	1.13	2.50	13	0.20
448	-23.70	4.18	16	0.96	2.19	11	0.16
451.8	-23.95	3.27	16	1.29	3.06	12	0.23
456	-24.71	4.42	15	0.76	2.46	15	0.19
460	-25.01	3.49	16	0.96	1.66	11	0.12
463.8	-23.70	4.42	17	1.23	0.64	5	0.04
468	-24.58	4.54	16	0.89	2.03	11	0.15
472	-23.63	4.76	16	1.14	1.69	12	0.13
475.8	-23.93	3.70	16	1.83	2.42	13	0.18
480	-24.65	5.52	17	1.45	1.12	8	0.08
484	-23.45	7.02	17	1.32	1.06	10	0.07
487.8	-24.06	4.55	17	1.64	1.43	16	0.10
492	-26.70	7.91	22	0.12	0.57	3	0.03
499.8	-25.56	6.12	18	2.98	3.63	11	0.24
504	-24.38	15.32	17	0.91	9.11	16	0.64
508	-24.04	7.12	13	0.62	1.66	6	0.15
512.55	-24.81	9.19	16	1.30	3.04	11	0.23
516	-24.75	11.27	15	0.88	4.89	19	0.37
520	-24.28	8.21	17	2.60	2.76	11	0.19
522.5	-24.23	10.41	15	1.30	3.71	10	0.29
528	-24.61	8.69	14	1.09	2.33	10	0.20
532	-25.68	5.89	13	1.28	2.20	14	0.20
535.5	-25.01	6.73	13	0.00	0.54	4	0.05
540	-25.47	6.70	13	0.76	1.13	7	0.10
544	-24.00	7.74	14	0.11	0.41	3	0.03
546.5	-25.38	8.23	16	0.59	4.30	16	0.32
552	-24.29	7.77	16	1.27	2.84	13	0.21
556	-23.83	6.85	14	0.77	3.88	19	0.31
559.5	-24.09	10.23	15	1.12	3.32	12	0.26
564	-24.13	8.38	18	0.57	1.87	8	0.12

Table 3: (Continued)

Depth (cm)	$\delta^{13}C_{ORG}$ (‰ VPDB)	$\delta^{15}N_{ORG}$ (‰ Air)	C:N (atomic)	TIC (wt. %)	TOC (wt. %)	BiSi (wt. %)	TN (wt. %)
568	-24.08	8.06	14	0.57	2.71	17	0.22
571.9	-24.55	9.01	15	0.87	2.88	14	0.23
576	-24.56	8.82	14	0.63	2.58	16	0.21
580	-25.41	6.54	14	1.29	2.30	13	0.19
583.5	-25.56	5.59	15	1.27	2.24	12	0.18
588	-24.41	7.97	15	0.47	2.58	21	0.27
592	-24.59	3.46	13	1.98	2.11	16	0.19
595.5	-25.30	4.14	14	1.30	2.02	14	0.17
600	-25.55	5.65	16	2.15	1.35	8	0.10
604	-23.02	6.41	16	0.56	0.82	6	0.06
607.5	-25.38	4.50	14	1.05	1.13	9	0.09
612	-25.81	5.97	12	1.51	1.02	11	0.10
616	-25.92	3.94	14	1.89	1.77	10	0.14
619.5	-25.53	4.56	14	0.64	1.23	10	0.10
624	-26.31	3.94	13	1.40	1.46	12	0.13
628	-26.28	5.71	12	1.11	1.66	17	0.15
631.5	-26.73	4.62	15	1.14	1.39	10	0.10
640	-26.76	6.17	12	1.28	1.84	17	0.17
643.5	-27.62	5.02	13	2.43	1.96	14	0.18
648	-26.45	6.64	12	2.49	2.66	19	0.25
652	-25.65	5.93	12	1.18	2.71	18	0.26
655.5	-26.15	4.53	13	0.44	1.37	10	0.13
660	-27.24	5.99	12	0.54	1.57	13	0.15
665.5	-27.44	4.71	14	0.40	1.11	11	0.09
668	-27.28	7.02	9	0.22	0.24	6	0.03
676	-27.42	4.69	13	0.85	1.00	13	0.09
680	-25.97	8.46	6	0.09	0.11	6	0.02
682.45	-28.29	3.78	13	0.56	1.40	16	0.13
692.45	-29.19	2.12	9	0.20	0.18	6	0.02
703.45	-25.53	3.89	14	0.49	0.41	4	0.03
732	-28.71	3.89	12	0.48	0.71	6	0.07
736	-28.34	5.03	13	0.40	0.53	6	0.05
740.25	-28.31	3.51	14	0.51	1.34	11	0.11
744	-29.92	4.98	13	0.67	1.49	13	0.13
748	-25.11	5.61	13	0.44	0.91	7	0.08
752.25	-26.50	4.22	12	0.57	1.27	17	0.13
756	-27.01	4.17	11	0.52	1.10	12	0.11
760	-29.15	4.97	15	0.68	1.63	12	0.13
764.25	-29.12	3.62	15	0.62	1.61	12	0.13
768	-27.15	4.45	13	0.53	1.03	10	0.09

Table 3: (Continued)

Depth (cm)	$\delta^{13}C_{ORG}$ (‰ VPDB)	$\delta^{15}N_{ORG}$ (‰ Air)	C:N (atomic)	TIC (wt. %)	TOC (wt. %)	BiSi (wt. %)	TN (wt. %)
772	-27.16	4.58	11	0.61	1.02	12	0.11
776.25	-28.07	3.87	13	0.62	1.10	12	0.10
780	-27.72	4.82	13	0.49	1.60	12	0.14
784	-26.38	3.77	12	0.53	1.34	14	0.14
788.25	-27.98	4.07	13	0.49	1.08	10	0.10
792	-28.87	5.55	11	0.43	1.23	11	0.13
796	-26.84	4.82	10	0.43	0.73	7	0.08
800.25	-26.60	4.50	13	0.43	1.15	10	0.10
804	-28.30	4.18	16	0.55	1.12	8	0.08
807	-29.47	3.36	18	0.49	1.13	9	0.07
812	-28.32	3.80	13	0.52	0.94	9	0.09
816	-26.85	3.20	11	0.58	1.05	14	0.11
819	-25.90	3.24	12	0.58	1.27	15	0.12
822	-25.98	7.23	11	0.56	0.98	9	0.11
828	-28.29	5.58	11	0.54	1.12	12	0.12
831	-29.26	2.98	15	0.56	1.22	8	0.10
836	-27.29	4.90	12	0.48	0.85	7	0.09
840	-25.67	5.27	16	0.45	1.07	9	0.08
843	-29.74	3.97	15	0.52	1.03	8	0.08
848	-25.97	6.62	8	0.48	0.35	5	0.05
852	-26.42	7.95	10	0.40	0.57	6	0.07
855	-25.82	4.97	38	0.38	2.53	7	0.08
860	-26.81	6.13	16	0.47	0.94	9	0.07
864	-26.59	6.12	10	0.52	0.35	4	0.04
867	-26.83	3.48	12	0.48	1.13	8	0.11
872	-27.30	5.18	12	0.51	0.80	9	0.08
876	-27.97	6.71	18	0.47	1.39	6	0.09
879	-26.87	5.46	10	0.48	0.75	8	0.08
884	-26.31	4.96	12	0.43	0.56	8	0.05
888	-22.25	6.56	11	0.42	0.50	7	0.06
891	-25.74	4.00	11	0.49	0.80	9	0.08
896	-26.23	9.79	11	0.41	0.37	3	0.04
900	-25.87	7.44	12	0.57	1.07	9	0.10
903	-25.10	9.13	12	1.24	1.07	8	0.10
908	-25.44	5.59	12	0.56	1.19	10	0.12
912	-27.32	5.56	12	0.53	1.14	11	0.11
915	-29.67	2.84	13	0.58	1.10	9	0.10
920	-27.17	5.61	12	0.55	1.16	9	0.12
924	-25.73	6.99	11	0.42	0.75	8	0.08
928	-24.30	7.39	9	0.32	0.16	2	0.02

Table 3: (Continued)

Depth (cm)	$\delta^{13}C_{ORG}$ (‰ VPDB)	$\delta^{15}N_{ORG}$ (‰ Air)	C:N (atomic)	TIC (wt. %)	TOC (wt. %)	BiSi (wt. %)	TN (wt. %)
932	-28.86	7.65	9	0.39	0.55	5	0.07
936	-27.08	5.14	10	0.40	0.56	6	0.06
940	-26.31	5.54	11	0.41	0.70	6	0.07
944	-24.09	5.30	10	0.42	0.64	6	0.07
948	-25.58	5.99	11	0.47	0.83	7	0.08
952	-27.23	5.61	10	0.53	0.74	6	0.09
956	-25.87	6.73	9	0.41	0.53	7	0.07
960	-25.50	7.73	13	0.51	0.63	7	0.06
964	-27.14	9.99	10	0.18	0.40	4	0.05
968	-22.09	9.84	12	0.28	1.92	13	0.18
972	-24.51	4.90	11	0.51	0.59	4	0.06
976	-26.46	6.36	10	0.55	0.48	5	0.05
980	-27.80	3.56	14	0.70	0.83	5	0.07
984	-27.55	5.48	13	0.70	0.77	5	0.07
988.9	-23.36	2.52	12	0.55	0.59	6	0.06
992	-26.90	3.59	14	0.63	0.95	8	0.08
996	-25.20	4.98	13	0.63	0.60	5	0.05
1000.9	-28.80	4.07	14	0.46	0.61	6	0.05
1004	-24.96	4.14	18	0.65	0.77	7	0.05
1008	-29.71	5.27	21	4.46	0.82	9	0.05
1012.9	-25.13	5.96	12	0.17	0.10	20	0.01
1024.9	-24.18	4.78	9	0.19	0.09	22	0.01
1028.9	-23.88	5.89	13	0.25	0.10	23	0.01
1055.9	-24.21	-2.93	N/A	0.00	0.13	17	0.00
1060.9	-26.75	-3.02	N/A	0.00	0.14	19	0.00

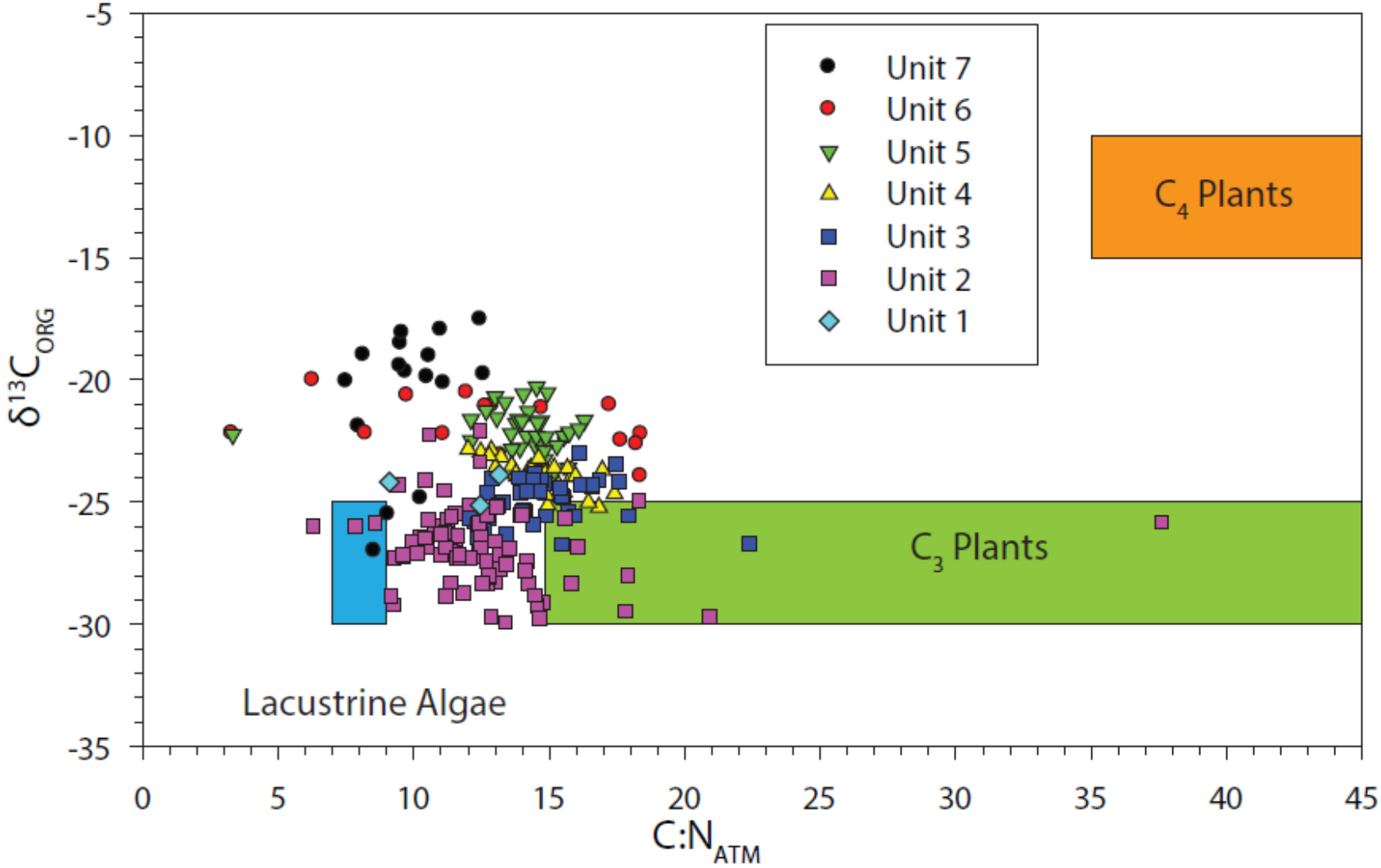

Figure 11: $C:N_{ATM}$ and $\delta^{13}C_{ORG}$ cross plot showing the dominant organic matter source(s) for each unit (modified from Meyers and Teranes, 2001). Note the up-section trend in source from lacustrine algae to C_3/C_4 plants and return to lacustrine algae.

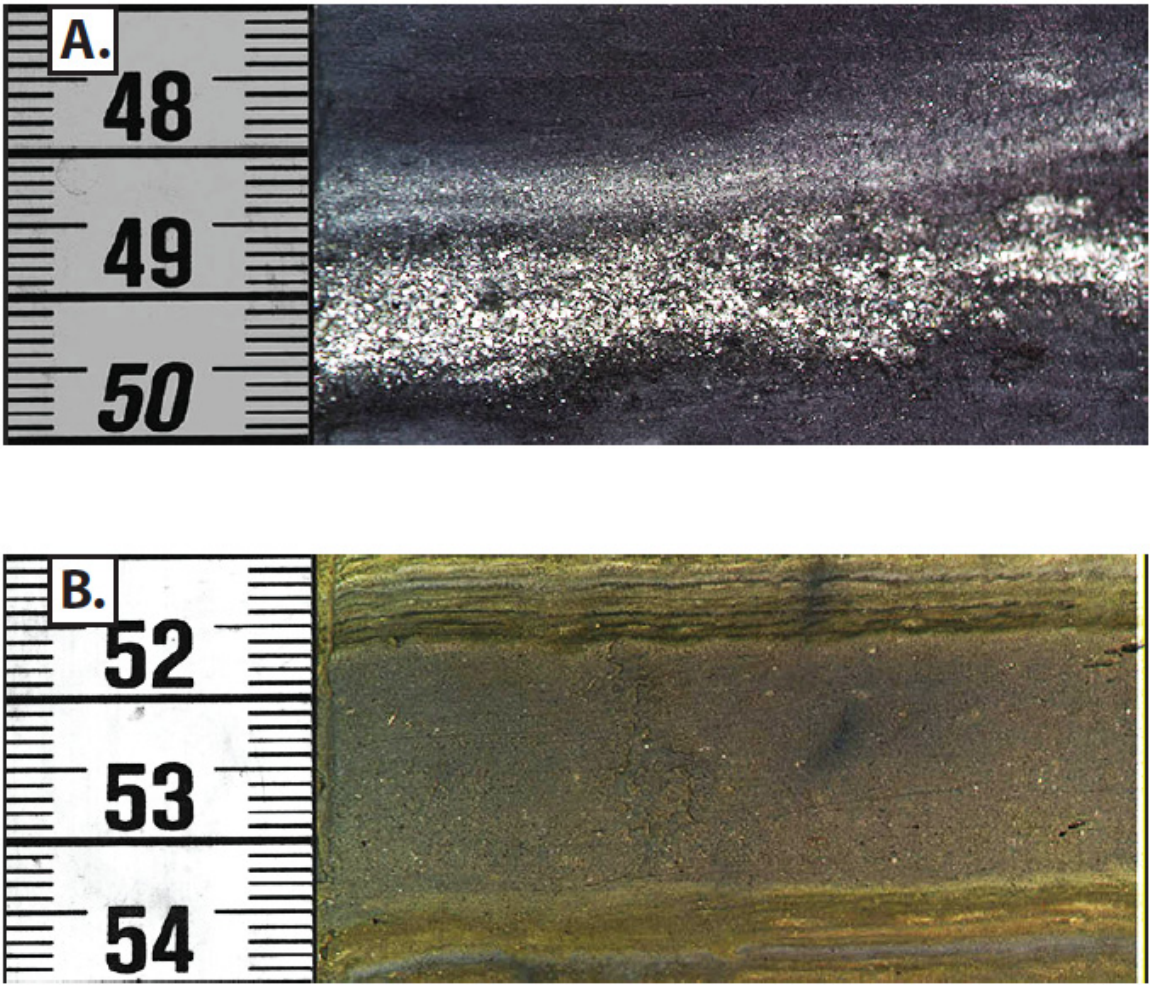

Figure 12: A: Lacustrine turbidite type 2 from the UWI15 core. Note the normal grading and predominance of siliciclastics. These turbidites are most common in the Pleistocene section due to deltaic progradation and riverine incision. B: Lacustrine turbidite type 1 from the UWI15 core, note the lack of a sandy base and siliciclastic component. These turbidites are dominantly composed of remobilized slope material.

CHAPTER SIX: CONCLUSIONS

- Data produced by this study support the hypothesis that organic-facies development over millennial time scales at Mono Lake is controlled by environmental changes. The study utilized a new ~11 m long piston core retrieved from deepwater (~18 m) using a percussion-piston coring device. Intact strata from Mono Lake are notoriously difficult to sample, due to the presence of multiple coarse tephra layers and disrupted intervals. The core utilized in this study is the first of its kind, and facilitates comparison with Mono Lake's well dated paleo-shoreline network for both the deglacial and late Holocene.

- A radiocarbon age model was developed for the core that relied on plant macrofossils, charcoal, and pollen purified by flow cytometry. The base of the core is believed to be ~16 ka; visual identification of late Pleistocene ash beds (Ash 1 and 2) helped to constrain this estimate. Although research is ongoing to improve the age model with additional pollen dates, the depositional history is currently well-understood for the Holocene and Pleistocene-Holocene transition. A large deposit of coarse pumice, potentially a debris flow initiated by earthquakes associated with the eruption of the South Mono tephra, generated an erosional unconformity that removed part of the late Holocene section (~4.2 ka -250 yr).

- The UWI15 core consists of a diverse sequence of laminated muds interbedded with tephras of varying thickness and texture. Seven units were identified in the core, based on variability in sedimentology, magnetic susceptibility (MS), elemental and stable isotope geochemistry. The sediments deposited during the Pleistocene deglacial are dominantly comprised of siliciclastic detritus (black clayey silts, cm-scale turbidites, and

occasional interbedded granitic sands and tephras) that produce high-amplitude, high-frequency MS variations. Laminated Holocene muds are characterized by low MS values, except for occasional turbidites and tephras, and range in color from a dark reddish-grey to olive-grey to a medium-brown.

- Paleo-shoreline data (Ali, 2018) suggest that two major highstands occurred at Mono Lake in the late Pleistocene: 18.5-16 ka and 12.9-11.7 ka (Younger Dryas). The older highstand is poorly represented in the UWI15 core, as those sediments were disrupted by the eruption of Black Point. In general, the chemostratigraphy of Pleistocene highstands is marked by low to moderate $C:N_{ATM}$, low to moderate TOC, moderate TIC, and moderate to high BiSi concentrations. The $\delta^{13}C_{ORG}$ trends toward enriched values, and the $\delta^{15}N_{ORG}$ trends toward depleted values. Comparatively, the Pleistocene lowstand ~16-12.9 ka are characterized by highly variable $C:N_{ATM}$, low TOC and TIC values, moderate BiSi concentrations, and $\delta^{13}C_{ORG}$ and $\delta^{15}N_{ORG}$ values are highly variable. During both the lowstand and highstands, the most influential factor on organic-facies development was dilution via the transport of glacial flour and riverine incision and deltaic progradation during lake level regressions >100 m. It is likely that turbidity associated with the influx of terrigenous sediments and ice-rafted debris limited the depth of light penetration, which acted as a constraint on photosynthetic organisms.

- Holocene highstands occurred at 10.9-8.7 ka and 6.3-4.2 ka and are characterized by moderate $C:N_{ATM}$ values, moderate-high TOC, moderate and stable TIC, and low-moderate BiSi concentrations. The $\delta^{13}C_{ORG}$ and $\delta^{15}N_{ORG}$ both trend towards depleted values during Holocene highstands. Lake-level lowstands occurred at 11.7-10.9 ka, 8.7-6.3 ka, and 250 yrs-present. Lowstands are characterized by low-moderate $C:N_{ATM}$

values, and highly variable TIC, TOC, and BiSi concentrations. The $\delta^{13}C_{ORG}$ and $\delta^{15}N_{ORG}$ both trend towards enriched values during lowstands, driven by changes in water chemistry and mixing. During the Holocene, organic-facies development was dominantly influenced by changes in wave base during regressions, which focused nearshore material downslope, and led to higher TIC (including nearshore carbonates like tufa flakes and ostracodes) and TOC (remobilized organic matter). Moreover, changes in lake level during the Holocene are minor (10's of meters) compared to Pleistocene lake-level changes (>100 m), as seen in the paleo-shoreline record generated by Ali (2018).

- Future work on the UWI15 work includes improvements to the age-depth model, palynological and ostracod analyses, build-up of thin-section data for additional ground truth of geochemistry using electron microprobe and microscope analyses, and non-destructive micron-scale scanning XRF analysis.

REFERENCES

Ali, G.A.H., 2018, Late Glacial and deglacial fluctuations of Mono Lake, California [Ph.D. thesis]: Columbia University, 255 p.

Bailey, R.A., Dalrymple, G.B., and Lanphere, M.A., 1976, Volcanism, structure, and geochronology of Long Valley Caldera, Mono County, California: Journal of Geophysical Research, v. 81, p. 725-744.

Baker, P.A., Seltzer., G.O., Fritz, S.C., Dunbar, R.B., Grove, M.J., Tapia, P.M., Cross, S.L., Rowe, H.D., and Broda, J.P., 2001, The history of South American tropical precipitation for the past 25,000 years: Science, v. 291, p. 640-643.

Baker, P.A. and Fritz, S.C., 2015, Nature and causes of Quaternary climate variation of tropical South America: Quaternary Science Reviews, v. 124, p. 31-47.

Barron, J.A., Metcalfe, S.E., and Addison, J.A., 2012, Response of the North American monsoon to regional changes in ocean surface temperature: Paleooceanography, v. 28, p. 1-17.

Bateman, P.C., 1961, Granitic formations in the east-central Sierra Nevada near Bishop, California: Geological Society of America Bulletin, v. 72, p. 1521-1538.

Benson, L.V., Currey, D.R., Dorn, R.I., Lajoie, K.R., Oviatt, C.G., Robinson, G.I., and Stine, S., 1990, Chronology of expansion and contraction of four Great Basin lake systems during the past 35,000 years: Palaeogeography, Palaeoclimatology, Palaeoecology, v. 78, p. 241-286.

Benson, L.V., Lund, S.P., Burdett, J.W., Kashgarian, M., Rose, T.P., Smoot, J.P., and Schwartz, M., 1997, Correlation of Late-Pleistocene lake-level oscillations in Mono Lake, California, with North Atlantic climate events: Quaternary Research, v. 49, p. 1-10.

Benson, L., Burdett, J., Lund, S., Kashgarian, M., and Mensing, S., 1997b, Nearly synchronous climate change in the Northern Hemisphere during the last glacial termination: Nature, v. 388, p. 263-265.

Benson, L.V., May, H.M., Antweiler, R.C., Brinton, T.I., Kashgarian, M., Smoot, J.P., and Lund, S.P., 1998, Continuous lake-sediment records in the Sierra Nevada between 52,600 and 12,500 ^{14}C yr B.P.: Quaternary Research, v. 50, p. 113-127.

Benson, L.V., Lund, S.P., Burdett, J.W., Kashgarian, M., Rose, T.P., Smoot, J.P., and Schwartz, M., 1998b, Correlation of Late-Pleistocene lake-level oscillations in Mono Lake, California, with North Atlantic Climate Events: Quaternary Research, v. 49, p. 1-10.

Benson, L., Kashgarian, M., Rye, R., Lund, S., and Paillet, F., 2002, Holocene multidecadal and multicentennial droughts affecting Northern California and Nevada; Quaternary Science Reviews, v. 21, p. 659-682.

Benson, L., Linsley, B., Smoot, J., Mensing, S., Lund, S., Stine, S., and Sarna-Wojcicki, A., 2003, Influence of the Pacific Decadal Oscillation on the climate of the Sierra Nevada, California and Nevada: Quaternary Research, v. 59, p. 151-159.

Benson, L., Lund, S., Negrini, R.M., Linsley, B., and Zic, M., 2003b, Response of North American Great Basin Lakes to Dansgaard-Oeschger oscillations: Quaternary Science Reviews, v. 22, p. 2,239-2,251.

Blaauw, M., and Christen, J.A., 2011, Flexible paleoclimate age-depth models using an autoregressive gamma process: Bayesian Analysis, v. 6, p. 457-474.

Bohacs, K.M., Carroll, A.R., Neal, J.E., and Mankiewicz, P.J., 2000, Lake-basin type, source potential, and hydrocarbon character: an integrated sequence-stratigraphic-geochemical framework, *in* E.H. Gierlowski-Kordesch and K.R. Kelts, eds., Lake basins through space and time: AAPG studies in Geology 46, p. 3-34.

Brasier, A., Wacey, D., Rogerson, M., Guagliardo, P., Saunders, M., Kellner, S., Mercedes-Martin, R., Prior, T., Taylor, C., Matthews, A., and Reijmer, J., 2018, A microbial role in the construction of Mono Lake carbonate chimneys?: Geobiology, https://doi.org/10.1111/gbi.12292

Bursik, M.I., and Gillespie, A.R., 1993, Late Pleistocene glaciation of Mono Basin, California: Quaternary Research, v. 39, p. 24-35.

Bursik, M., Renshaw, C., McCalpin, J., and Berry, M., 2003, A volcanotectonic cascade: Activation of range front faulting and eruptions by dike intrusion, Mono Basin-Long Valley Caldera, California: Journal of Geophysical Research, v. 108, p. 10.1-10.14.

Bursik, M., Sieh, K., and Meltzner, A., 2014, Deposits of the most recent eruption in the Southern Mono Craters, California: Description, interpretation and implications for regional marker tephras: Journal of Volcanology and Geothermal Research, v. 275, p. 114-131.

Chiang, J.C.H., Lee, S., Putnam, A.E., and Wang, X., 2014, South Pacific Split Jet, ITCZ shifts, and atmospheric North-South linkages during abrupt climate changes of the last glacial period: Earth and Planetary Science Letters, v. 406, p. 233-246.

Christensen, M.N., Gilbert, C.M., Lajoie, K.R., and Al-Rawi, Y., 1969, Geological-geophysical interpretation of Mono Basin, California-Nevada: Journal of Geophysical Research, v. 74, p. 5221-5239.

Cohen, A.S., 2003, Paleolimnology: New York, Oxford University Press Inc., 500 p.

COHMAP, 1988, Climate changes of the last 18,000 yr: Observations and model simulations: Science, v. 241, p. 1043-1052.

Colman, S.M., Yua, S., Anc, A., Shend, J., Henderson, A.C.G., 2007, Late Cenozoic climate changes in China's western interior: A review of research on Lake Quinghai and comparison with other records: Quaternary Science Reviews, v. 26, p. 2281-2300.

Colman, S.M., Hemming, S.R., Stine, S., and Zimmerman, S.R.H., 2014, The effects of recent uplift and volcanism on deposition in Mono Lake, California, from seismic-reflection (CHIRP) profiles: Journal of Geophysical Research: Solid Earth, v. 119, p. 1-16.

Cook, E.R., Seager, R., Heim, R.R., Vose, R.S., Herweijer, C., and Woodhouse, C., 2009, Megadroughts in North America: placing IPCC projections of hydroclimate change in a long-term palaeoclimate context: Journal of Quaternary Science, v. 25, p. 48-61.

Cvijanovic, I., Santer, B.D., Bonfils, C., Lucas, D.D., Chiang, J.C.H., and Zimmerman, S., 2017, Future loss of Arctic sea-ice cover could drive a substantial decrease in California's rainfall: Nature Communications, v. 8:1947, p. 1-10.

Davis, O.K., and Moutoux, T.E., 1998, Tertiary and Quaternary vegetation history of the Great Salt Lake, Utah, USA: Journal of Paleolimnology, v. 19, p. 417-427.

Davis, O.K., 1999, Pollen analysis of a late glacial and Holocene sediment core from Mono Lake, Mono County, California: Quaternary Research, v. 52, p. 243-249.

Denton, G.H., Broecker, W.S., and Alley, R.B., 2006, The mystery interval 17.5 to 14.5 kyrs ago: PAGES News, v. 14, p. 14-16.

Ellis, G.S., Katz, B.J., Scholz, C.A., and Swart, P.K., 2015, Organic sedimentation in modern lacustrine systems: A case study from Lake Malawi, East Africa, *in* Larsen, D., Egenhoff, S.O., and Fishman, N.S., eds., Paying Attention to Mudrocks: Priceless!: Geological Society of America Special Paper 515, p. 19-47, doi: 10.1130/2015.2515(02).

Forester, R.M., 1987. Late Quaternary paleoclimate records from lacustrine ostracods. In: Ruddiman, W.F., Wright, H.E. Jr. (Eds.), North America and adjacent Ocean during the Last Glaciation. The Geology of North America, Vol. K-3, Geological Society of America, Boulder, CO, pp. 261–276.

Fritz, S.C., Engstrom, D.R., and Juggins, S., 2004, Patterns of early lake evolution in boreal landscapes: a comparison of stratigraphic inferences with a modern chronosequence in Glacier Bay, Alaska: The Holocene, v. 14:6, p. 828-840.

Garrels, R.M., and Mackenzie, F.T., 1967, Origin of the chemical compositions of some springs and lakes: Advances in Chemistry, v. 67, p. 222-242.

Godsey, H.S., Oviatt, C.G., Miller, D.M., and Chan, M.A., 2011, Stratigraphy and chronology of offshore to nearshore deposits associated with the Provo shoreline, Pleistocene Lake Bonneville, Utah: Palaeogeography, Palaeoclimatology, Palaeoecology, v. 310, p. 442-450.

Griffin, D., and Anchukaitis, K.J., 2014, How unusual is the 2012-2014 California drought?: Geophysical Research Letters, v.41, p. 9017-9023.

Guyard, H., St-Onge, G., Pienits, R., Francus, P., Zolitschka, B., Clark, G.K.C., Hausmann, S., Salonen, V.P., Lajeunesse, P., Ledoux, G., and Lamothe, M., 2011, New insights into Late Pleistocene glacial and post glacial history of northernmost Ungava (Canada) from Pingualuit Crater Lake sediments: Quaternary Science Reviews, v. 30, p. 3892-3907.

Hecky, R.E., Bootsma, H.A., Mugidde, R.M., Bugenyi, F.W.B., Phosphorous pumps, nitrogen sinks, and silicon drains: plumbing nutrients in the African Great Lakes *in* Johnson, I.C.., Odada, E.O., editors, The Limnology, climatology and paleontology of east African Lakes: Amsterdam: Gordon and Breach; 1996, p. 205-234.

Herbst, D.B., and Blinn, D.W., 1998, Experimental mesocosm studies of salinity effects on the benthic algal community of a saline lake: Journal of Phycology, v. 34, p. 772-778.

Herweijer, C., Seager, R., Cook, E.R., and Emile-Geay, J., 2007, North American droughts of the last millennium from a gridded network of tree-ring data: American Meteorological Society, v. 20, p. 1353-1376.

Hildreth, W., 2004, Volcanological perspectives on Long Valley, Mammoth Mountain, and Mono Craters: several contiguous but discrete systems: Journal of Volcanology and Geothermal Research, v. 136, p. 169-198.

Jellison, R., and Melack, J., 1993, Algal photosynthetic activity and its response to meromixis in hypersaline Mono Lake, California: American Society of Limnology and Oceanography, v. 38(4), p. 818-837.

Jellison, R., and Melack, J.M., 1993b, Meromixis in hypersaline Mono Lake, California 1. Stratification and vertical mixing during the onset, persistence, and breakdown of meromixis: American Society of Limnology and Oceanography, v. 38(5), p. 1008-1019.

Jellison, R., Miller, L.G., Melack, J.M., and Dana, G.L., 1993, Meromixis in hypersaline Mono Lake, California. 2. Nitrogen fluxes: American Society of Limnology and Oceanography, v. 38(5), p. 1020-1039.

Jellison, R., Anderson, R.F., Melack, J.M., and Heil, D., 1996, Organic Matter accumulation in sediments of hypersaline Mono Lake during a period of changing salinity: Limnology and oceanography, v. 41(7), p. 1539-1544.

Jones, B.F., and Deocampo, D.M., 2003, Geochemistry of saline lakes: Treatise on Geochemistry, v. 5, p. 393-424.

Kelleher, P.C., and Cameron, K.L., 1990, The geochemistry of the Mono craters-Mono Lake islands volcanic complex, eastern California: Journal of Geophysical Research, v. 95, p. 17643-17659.

Kociolek, J.P., and Herbst, D.B., 1992, Taxonomy and distribution of benthic diatoms from Mono Lake, California, U.S.A.: Transactions of the American Microscopial Society, v. 111, p. 338-355.

Koehler, C.L., 1995, Water rights and the public trust doctrine: resolution of the Mono Lake Controversy: Ecology Law Quarterly, v. 22, p. 541-589.

Laird, K.R., Fritz, S.C., Grimm, E.C., and Mueller, P.G., 1996, Century-scale paleoclimatic reconstruction from Moon Lake, a closed-basin lake in northern Great Plains: Limnology and Oceanography, v. 41(5), p. 890-902.

Lajoie, K.R., 1968, Quaternary stratigraphy and geologic history of Mono Basin, Eastern California [Ph.D. thesis]: University of California, 383 p.

Lascu, I., 2009, Magnetic Susceptibility Core Logging: http://lrc.geo.umn.edu/laccore/icd.html (accessed November 2017).

Liu, Z., Otto-Bliesner, B.L., He, F., Brady, E.C., Tomas, R., Clark, P.U., Carlson, A.E., Lynch-Stieglitz, J., Curry, W., Brook, E., Erickson, D., Jacob, R., Kutzbach, J., and Cheng, J., 2009, Transient simulation of last deglaciation with a new mechanism for Bolling-Allerod warming: Science, v. 325, p. 310-314.

Lowenstein, T.K., Brown, C., Roberts, S.M., Ku, T., Luo, S., and Yang, W., 1999, 200 k.y. paleoclimate record from Death Valley salt core: Geology, v.27, p. 3-6.

MacDonald, G.M., Moser, K.A., Bloom, A.M., Porinchu, D.F., Potito, A.P., Wolfe, B.B., Edwards, T.W.D., Petel, A., Orme, A.R., and Orme, A.J., 2008, Evidence of temperature depression and hydrological variations in the eastern Sierra Nevada during the Younger Dryas stade: Quaternary Research, v. 70, p. 131-140.

MacIntyre, S., Flynn, K.M., Jellison, R., and Romero, J.R., 1999, Boundary mixing and nutrient fluxes in Mono Lake, California: American Society of Limnology and Oceanography, v. 44(3), p. 512-529.

Marcaida, M., Mangan, M.T., Vazquez, J.A., Bursik, M., and Lidzbarski, M.I., 2014, Geochemical fingerprinting of Wilson Creek Formation tephra layers (Mono Basin, California) using titanomagnetite compositions: Journal of Volcanology and Geothermal Research, v. 273, p. 1-14.

McFadden, M.A., Mullins, H.T., Patterson, W.P., and Anderson, W.T., 2004, Paleoproductivity of eastern Lake Ontario over the past 10,000 years: American Society of Limnology and Oceanography, v. 49(5), p. 1570-1581.

McGlue, M.M., Scholz, C.A., Karp, T., Ongodia, B., and Lezzar, K.E., 2006, Facies architecture of flexural margin lowstand delta deposits in Lake Edward, East African Rift: Constraints from seismic reflection imaging: Journal of Sedimentary Research, v. 76, p. 942-958.

McGlue, M.M., Silva, A., Zani, H., Corradini, F.A., Parolin, M., Abel, E.J., Cohen, A.S., Assine, M.L., Ellis, G.S., Trees, M.A., Kuerten, S., Santos Gradella, F., and Rasbold, G.G., 2012, Lacustrine records of Holocene flood pulse dynamics in the Upper Paraguay River watershed (Pantanal wetlands, Brazil): Quaternary Research, v. 78, p. 285-294.

Mensing, S.A., 2001, Late-Glacial and Early Holocene vegetation and climate change near Owens Lake, Eastern California: Quaternary Research, v. 55, p. 57-65.

Mensing, S.A., Benson, L., Kashgarian, M., and Lund, S., 2004, A Holocene pollen record of persistent droughts from Pyramid Lake, Nevada, USA: Quaternary Research, v. 62, p. 29-38.

Meyers, P.A., and Lallier-Verges, E., 1999, Lacustrine sedimentary organicmatter records of Late Quaternary paleoclimates: Journal of Paleolimnology, v. 21, p. 345-372.

Meyers, P.A., and Teranes, J.L., 2001, Sediment organic matter, *in* Last, W.M., and Smol, J.P., ed., Tracking environmental change using lake sediments: Dordrecht, Netherlands, Kluwer Academic Publishers, v. 2, p. 239- 269.

Meyers, P.A., 2002, Evidence of mid-Holocene climate instability from variations in carbon burial in Seneca Lake, New York: Journal of Paleolimnology, v. 28, p. 237-244.

Meyers, P.A., 2003, Applications of organic geochemistry to paleolimnological reconstructions: a summary of examples from the Laurentian Great Lakes: Organic Geochemistry, v. 34, p. 261-289.

Middleton, G.V., and Hampton, M.A., 1973, Sediment gravity flows: mechanics of flow and deposition *in* Turbidity and Deep Water Sedimentation (Eds G.V. Middleton and A.H. Bouma), SEPM, Pacific section, short course lecture notes, 1-38.

Millar, C.I., King, J.C., Westfall, R.D., Alden, H.A., and Delany, D.L., 2006, Late Holocene forest dynamics, volcanism, and climate change at Whitewing Mountain and San Joaquin Ridge, Mono County, Sierra Nevada, CA, USA: Quaternary Research, v. 66, p. 273-287.

Moernaut, J., Van Daele, M., Heirman, K., Fontijin, K., Strasser, M., Pino, M., Urrutia, R., and Batist, M., 2014, Lacustrine turbidites as a tool for quantitative earthquake reconstruction: New evidence for a variable rupture mode in south central Chile: Journal of Geophysical Research: Solid Earth, v. 119, doi: 10.1002/2013JB010738.

Morrissey, A., and Scholz, C.A., 2014, Paleohydrology of Lake Turkana and its influence on the Nile River System: Palaeogeography, Palaeoclimatology, Palaeoecology, v. 403, p, 88-100.

Mortlock, R.A., and Froelich, P.N., 1989, A simple method for the rapid determination of biogenic opal in pelagic marine sediments: Deep-Sea Research, v. 36, p. 1,415-1,426.
Newton, M.S., 1994, Holocene fluctuations of Mono Lake, California: The sedimentary record: Society for Sedimentary Geology Special Publication, v. 50, p. 143-157.
Noble, P.J., Ball, G.I., Zimmerman, S.H., Maloney, J., Smith, S.B., Kent, G., Adams, K.D., Karlin, R.E., and Driscoll, N., 2016, Holocene paleoclimate history of Fallen Leaf Lake, CA., from geochemistry and sedimentology of well-dated sediment cores: Quaternary Science Reviews, v. 131, p. 193-210.
Nowak, R.S., Nowak, C.L., and Tausch, R.J., 2017, Vegetation dynamics during last 35,000 years at a cold desert locale: preferential loss of forbs with increased aridity: Ecosphere, v. 8(7), p. 1-23.
Obbink, E.A., Carlson, A.E., and Klinkhammer, G.P., 2010, Eastern North American freshwater discharge during the Bolling-Allerod warm periods: Geology, v. 38, p. 171-174.
Olsen, M.S., Callaghan, T. V., Reist, J.D., Reiersen, L.O., Dahl-Jensen, D., Granskog, M.A., Goodison, B., Hovelsrud, G.K., Johansson, M., Kallenborn, R., Key, J., Klepikov, A., Meier, W., Overland, J.E., Prowse, T. D., Sharp, M., Vincent, W.F., and Walsh, V.J., 2011, The changing Arctic cryosphere and likely consequences: An overview: AMBIO, v. 40, p. 111-118.
Oremland, R.S., Miller, L.G., and Whiticar, M.J., 1987, Sources and flux of natural gases from Mono Lake, California: Geochinica et Cosnochimica Acta, v. 51, p. 2915-2929.
Osleger, D.A., Heyvaert, A.C., Stoner, J.S., and Verosub, K.L., 2008, Lacustrine turbidites as indicators of Holocene storminess and climate: Lake Tahoe, California and Nevada: Article *in* Journal of Paleolimnology, DOI: 10.1007/s10933-008-9265-8.
Oviatt, C.G., 1997, Lake Bonneville fluctuations and global climate change: Geology, v. 25, p. 155-158.
Page, G.W., Stenzel, L.E., Winkler, D.W., and Swarth, C.W., 1983, Spacing out at Mono Lake: Breeding success, nest density, and predation in the Snowy Plover: The Auk, v. 100, p. 13-24.
Pedersen, R.A., Cvijanovic, I., Langen, P.L., and Vinther, B.M., 2016, The impact of regional Arctic sea ice loss on atmospheric circulation and the NAO: American Meteorological Society, v. 29, p. 889-902.
Placzek, C., Quade, J., and Patchett, J.P., 2006, Geochronology and stratigraphy of late Pleistocene lake cycles on the southern Bolivian Altiplano: Implications for causes of tropical climate change: GSA Bulletin, v. 118, p. 515-532.
Placzek, C.J., Quade, J., and Patchett, P.J., 2013, A 130 ka reconstruction of rainfall on the Bolivian Altiplano: Earth and Planetary Science letters, v. 363, p. 97-108.
Potter, P.E., Maynard, J.B., and Depetris, P.J., 2005, Mud and mudstones: Introduction and overview: Berlin, Germany, Springer, 304 p.
Qiu, L., Williams, D.F., Gvorzdkov, A., Karabanov, E., and Shimaraeva, M., 1993, Biogenic silica accumulation and paleoproductivity in the northern basin of Lake Baikal during the Holocene: Geology, v. 21, p. 25-28.

Reed, W.E., 1977, Biogeochemistry of Mono Lake, California: Geochimica et Cosmochimica Acta, v. 41, p. 1231-1245.
Reheis, M.C., Stine, S., and Sarna-Wojcicki, A.M., 2002, Drainage reversals in Mono Basin during the late Pliocene and Pleistocene: GSA Bulletin, v. 114, p. 991-1006.
Respaut, R., 2016, Business News: California surpasses France as worlds sixth largest economy: http://www.reuters.com (accessed December 2016). http://www.reuters.com/article/us-california-economy-idUSKCN0Z32K2
Schnurrenberger, D., Russell, J., and Kelts, K., 2003, Classification of lacustrine sediments based on sedimentary components: Journal of Paleolimnology, v. 29, p. 141-154.
Shakun, J.D., Clark, P.U., He, F., Marcott, S.A., Mix, A.C., Liu, Z., Otto-Bliesner, B., Schmittner, A., and Bard, E., 2012, Global warming preceded by increasing carbon dioxide concentrations during the last deglaciation: Nature, v. 484, p. 49-55.
Shanahan, T.M., Overpeck, J.T., Wheeler, C.W., Beck, J.W., Pigati, J.S., Talbot, M.R., Sholz, C.A., Peck, J., and King, J.W., 2006, Paleoclimatic variations in West Africa from a record of late Pleistocene and Holocene lake level stands of Lake Bosumtwi, Ghana: Palaeogeography, Palaeoclimatology, Palaeoecology, v. 242, p. 287-302.
Sierra Nevada Conservancy, 2015, California's Primary Watershed: http://www.sierranevada.ca.gov//our-region/ca-primary-watershed (accessed March 2018).
Stine, S., 1987, Mono Lake: The past 4,000 years [Ph.D. thesis]: Berkeley, University of California, 859 p.
Stine, S., 1990, Late Holocene fluctuations of Mono Lake, eastern California: Palaeogeography, Palaeoclimatology, Palaeoecology, v. 78, p. 333-381.
Stine, S., 1991, Geomorphic, geographic, and hydrographic basis for resolving the Mono Lake Controversy: Environmental Geology and Water Sciences, v. 17, p. 67-83.
Talbot, M.R., and Johannessen, T., 1992, A high resolution palaeoclimatic record for the last 27,500 years in tropical West Africa from the carbon and nitrogen isotopic composition of lacustrine organic matter: Earth and Planetary Science Letters, v. 110, p. 23-37.
Tenzer, G.B., Meyers, P.A., and Knoop, P., 1997, Sources and distribution of organic and carbonate carbon in surface sediments of Pyramid Lake, Nevada: Journal of Sedimentary Research, v. 67, p. 884-890.
Tunno, I., and Mensing, S.A., 2017, The value of non-pollen palynomorphs in interpreting paleoecological change in the Great Basin (Nevada, USA): Quaternary Research, v. 87, p. 529-543.
Van Daele, M., Moernaut, J., Doom, L., Boes, E., Fontijn, K., Heirman, K., Vandoorne, W., Hebbeln, D., Pino, M., Urrutia, R., Brummer, R., and Batist, M., 2015, A comparison of the sedimentary records of the 1960-210 great Chilean earthquakes in 17 lakes: Implications for quantitative lacustrine palaeoseismology: Sedimentology, v. 62, p. 1466-1496.

Vazquez, J.A., and Lidzbarski, M.I., 2012, High-resolution tephrochronology of the Wilson Creek Formation (Mono Lake, California) and Laschamp event using ^{238}U-^{230}Th SIMS dating of accessory mineral rims: Earth and Planetary Science Letters, v. 357, p. 54-67.

Vicuna, S., and Dracup, J.A., 2007, The evolution of climate change impact studies on hydrology and water resources in California: Climatic Change, v. 82, p. 327-350.

Wang, M., and Overland, J.E., 2009, A sea ice free summer Arctic within 30 years?: Geophyiscal Research Letters, v. 36, p. 1-5.

Weaver, A. J., Saenko, O.A., Clark, P.U., and Mitrovica, J.X., 2003, Meltwater Pulse 1A form Antarctica as a trigger of the Bolling-Allerod warm interval: Science, v. 299, p. 1709-1713.

Wetzel, R.G., 2001, Limnology: Lake and River Ecosystems: 3rd ed. Academic Press, San Diego, California, USA.

Wiens, J.A., Patten, D.T., and Botkin, D.B., 1993, Assessing ecological impact assessment: Lessons from Mono Lake, California: Ecological Applications, v. 3, p. 595-609.

Wood, S.H., 1977, Distribution, correlation, and radiocarbon dating of late Holocene tephra, Mono and Inyo craters, eastern California: Geological Society of America Bulletin, v. 88, p. 89-95.

Wrege, P.H., Shuford, W.D., Winkler, D.W., and Jellison, R., 2006, Annual variation in numbers of breeding California Gulls at Mono Lake, California: The importance of natal philopatry and local and regional conditions: The Condor, v.108, p. 82-96.

Zimmerman, S.H., Hemming, S.R., Kent, D.V., Searle, S.Y., 2006, Revised chronology for late Pleistocene Mono Lake sediments based on paleointensity correlation to the global reference curve: Earth and Planetary Science Letters, v. 252, p. 94-106.

Zimmerman, S.R.H., Hemming, S.R, Hemming, N.G., Tomascak, P.B., and Pearl, C., 2011, High-resolution chemostratigraphic record of late Pleistocene lake-level variability, Mono Lake, California: Geological Society of America Bulletin, v. 123, p. 2320-2334.

Zimmerman, S.H., Pearl, C., Hemming, S.R., Tamulonis, K., Hemming, N.G., and Searle, S.Y., 2011b, Freshwater control of ice-rafted debris in the last glacial period at Mono Lake, California, USA: Quaternary Research, v. 76, p. 264-271.

Zimmerman, S., and Myrbo, A., 2015, Lacustrine environments (^{14}C). In: Jack Rink W., Thompson J.W., (eds) Encyclopedia of Scientific Dating Methods. Encyclopedia of Earth Sciences Series. Springer, Dordrecht.

Zimmerman, S.H., Hemming, S., and Starratt, S., 2018, Holocene sedimentary architecture and paleoclimate variability at Mono Lake, CA, from multiple sediment cores: GSA Books, (in rev.).

VITA

Bailee Nicole Hodelka

Louisville, Kentucky

Education

B.A. Geological Sciences (2014)

University of Kentucky

Experience

Graduate Teaching Assistant

Department of Earth and Environmental Sciences

University of Kentucky, 40506

Graduate Research Assistant

Pioneer Paleoenvironments and Stratigraphy Lab

Department of Earth and Environmental Sciences

University of Kentucky, 40506

Student Geologist

Kentucky Geological Survey

University of Kentucky, 40506

Undergraduate Researcher

Department of Earth and Environmental Sciences

University of Kentucky, 40506

Laboratory Technician

Department of Earth and Environmental Sciences

University of Kentucky, 40506